© 2020. Published by The Company of Biologists Ltd | Journal of Cell Science (2020) 133, jcs232405. doi:10.1242/jcs.232405

RESEARCH ARTICLE

SPECIAL ISSUE: CELL BIOLOGY OF THE IMMUNE SYSTEM

Adhesion, motility and matrix-degrading gene expression changes in CSF-1-induced mouse macrophage differentiation

Michael W. Murrey[1,*], James H. Steer[2,*], Eloise L. Greenland[1], Julie M. Proudfoot[1], David A. Joyce[2] and Fiona J. Pixley[1,‡]

ABSTRACT

Migratory macrophages play critical roles in tissue development, homeostasis and disease, so it is important to understand how their migration machinery is regulated. Whole-transcriptome sequencing revealed that CSF-1-stimulated differentiation of bone marrow-derived precursors into mature macrophages is accompanied by widespread, profound changes in the expression of genes regulating adhesion, actin cytoskeletal remodeling and extracellular matrix degradation. Significantly altered expression of almost 40% of adhesion genes, 60–86% of Rho family GTPases, their regulators and effectors and over 70% of extracellular proteases occurred. The gene expression changes were mirrored by changes in macrophage adhesion associated with increases in motility and matrix-degrading capacity. IL-4 further increased motility and matrix-degrading capacity in mature macrophages, with additional changes in migration machinery gene expression. Finally, siRNA-induced reductions in the expression of the core adhesion proteins paxillin and leupaxin decreased macrophage spreading and the number of adhesions, with distinct effects on adhesion and their distribution, and on matrix degradation. Together, the datasets provide an important resource to increase our understanding of the regulation of migration in macrophages and to develop therapies targeting disease-enhancing macrophages.

KEY WORDS: CSF-1, Interstitial motility, Paxillin, Leupaxin, IL-4

INTRODUCTION

Tissue macrophages are resident chameleons that finely tune their phenotype to adapt to the local demands of their tissue of residence (Gautier et al., 2012). For example, Kupffer cells in the liver are quite different to peritoneal or splenic macrophages or brain microglia. Further diversity is derived from the developmental origin of the precursor. While most tissue macrophages, including Kupffer cells and microglia, originate from embryonically derived progenitor cells, intestinal macrophages are largely derived from hematopoietic stem cells in the adult bone marrow (Perdiguero and Geissmann, 2015). Nevertheless, these different macrophage populations all perform common duties such as immune surveillance and injury repair along with their specialized tissue-specific functions (Okabe and Medzhitov, 2015). Similarly, most macrophage populations depend on the colony stimulating factor-1 (CSF-1)–CSF-1 receptor (CSF-1R) axis for their establishment and survival in different tissues (Wynn et al., 2013; Sullivan and Pixley, 2014). The reliance of developing and homeostatic macrophages on CSF-1R signaling is reflected in the recommendation that CSF-1-differentiated bone marrow-derived macrophages (BMMs) be considered the *in vitro* baseline standard for mouse macrophage experimentation (Murray et al., 2014).

The CSF-1R is a class III receptor tyrosine kinase that triggers a range of signaling pathways in BMMs and precursor mononuclear phagocytic cells (Sullivan and Pixley, 2014). It is activated by two ligands, CSF-1 and interleukin (IL)-34, which have different spatiotemporal expression patterns (Wei et al., 2010). However, whereas the CSF-1-deficient osteopetrotic mouse has many developmental defects due to reductions in tissue macrophage populations, the IL-34-deficient mouse is essentially normal, indicating that CSF-1 is the primary macrophage growth factor (Sullivan and Pixley, 2014). CSF-1 is also important for tissue homeostasis in the adult mouse through support of tissue macrophage populations (Wynn et al., 2013). The pleiotropic signaling of the CSF-1R makes it difficult to delineate signals specific to the CSF-1–CSF-1R axis. However, although other cytokines such as granulocyte-macrophage (GM)-CSF (also known as CSF-2) support macrophage survival and proliferation, CSF-1 appears to play a non-redundant role in the differentiation of macrophage precursor cells into mature adherent macrophages capable of interstitial migration (Yu et al., 2008; Pixley and Stanley, 2004; Pixley, 2012).

Cells adhere to underlying extracellular matrix (ECM) proteins through integrin-mediated adhesions, which consist of large numbers of proteins residing in or regulating the assembly and disassembly of these dynamic connections to the intracellular actin cytoskeleton. A bioinformatics approach was used to assemble an adhesome of 232 proteins categorized into adhesion receptors, adaptor proteins, actin regulators and other proteins (Winograd-Katz et al., 2014). A subsequent meta-analysis of fibronectin-induced adhesion proteins increased the list to more than 2400 proteins, from which a ‘consensus adhesome’ of 60 proteins found in at least five different cell types was determined (Horton et al., 2015). Finally, a compartmentalized network of 258 proteins was derived from the consensus and literature-curated adhesomes (Horton et al., 2016). As macrophages form tiny dot-like point contacts and small linear focal complexes rather than larger focal adhesions typical of other mesenchymal cells, the adhesome in mature macrophages contains additional selectively expressed proteins (Pixley, 2012). This is exemplified by their expression of two adhesion kinases, focal adhesion kinase (FAK; also known as PTK2) and Pyk2 (also known as PTK2B), and five Src family kinases (SFKs), Src, Fyn, Hck, Fgr and Lyn, to coordinate phosphorylation on tyrosine of many adhesion proteins during adhesion turnover and signaling (Dwyer et al., 2016; Zaidel-Bar et al., 2007; Owen et al., 2007; Abram and Lowell, 2008). Macrophages also form podosomes, which have both adhesion and

[1]School of Biomedical Sciences, Faculty of Health and Medical Sciences, The University of Western Australia, 35 Stirling Highway, Crawley, WA 6009, Australia. [2]Medical School, Faculty of Health and Medical Sciences, The University of Western Australia, 35 Stirling Highway, Crawley, WA 6009, Australia.
*These authors contributed equally to this work

‡Author for correspondence (fiona.pixley@uwa.edu.au)

F.J.P., 0000-0002-1571-2532

Received 27 March 2019; Accepted 17 January 2020

Journal of Cell Science (2020) 133, jcs232405. doi:10.1242/jcs.232405

matrix-degrading functions, and commonly organize into circular rosettes in mouse macrophages (Dwyer et al., 2016; Linder and Wiesner, 2015).

Cell migration requires the co-regulation of cell adhesion with actin polymerization and acto-myosin contractility (Lauffenburger and Horwitz, 1996; Devreotes and Horwitz, 2015). Rho family GTPases are key regulators of the actin cytoskeleton (Bustelo et al., 2007; Ridley, 2011). Grouped by structural similarities, they are tightly regulated themselves by activators, guanine nucleotide exchange factors (GEFs), and two groups of inactivators, GTPase activating proteins (GAPs) and Rho-GDP dissociation inhibitors (Bustelo et al., 2007; Ridley, 2011). To move through the interstitial space of tissues, macrophages recruit extracellular proteases to podosomes (Linder and Wiesner, 2015). The ECM proteases implicated in macrophage interstitial migration are matrix metalloproteinases (MMPs), cathepsins and urokinase-type plasminogen activator (uPa; also known as Plau) (Vérollet et al., 2011).

Baseline mature macrophages differentiated in the presence of CSF-1 can be further activated by cytokines. Although *in vivo* cytokines produce a mix of activated macrophage phenotypes, a linear range of activation from interferon (IFN)-γ-induced classically activated 'M1' macrophages through to IL-4-induced alternatively activated 'M2' macrophages is a commonly cited concept (Xue et al., 2014; Mosser and Edwards, 2008). Macrophage activation is particularly important in the context of disease as macrophages can be subverted to contribute to disease progression (Wynn et al., 2013). Notably, tumor-associated macrophages (TAMs) promote tumor progression in a number of ways (Yang et al., 2018). CSF-1R signaling in TAMs appears to play a critical role in tumor invasion and metastasis, as revealed in a mouse model of breast cancer (Lin et al., 2001). In this model, tumor cells and TAMs participated in a paracrine CSF-1–epidermal growth factor (EGF) loop, leading to their co-migration, invasion and metastasis (Wyckoff et al., 2004). TAMs are thought to predominantly adopt an alternatively activated or M2-like phenotype, and IL-4 has been shown to skew TAMs towards this tumor-promoting state (DeNardo et al., 2009).

As CSF-1 is a critical regulator of macrophage adhesion, migration and invasive capacity *in vitro* and *in vivo* (Wyckoff et al., 2004; Webb et al., 1996; Pixley et al., 2001), it is important to delineate the mechanisms by which CSF-1 regulates the development of these functions. Similarly, further characterization of tumor-promoting changes induced by IL-4 in TAMs may help to identify therapeutic targets to inhibit tumor invasion and metastasis. CSF-1 rapidly triggers BMM spreading, adhesion and motility through CSF-1R pY721-activated phosphatidylinositol 3-kinase (PI3K) p110δ (also known as PIK3CD) (Sampaio et al., 2011; Mouchemore et al., 2013), and also regulates macrophage adhesion and migration in the longer term through SFK gene expression changes via CSF-1R pY974 (Dwyer et al., 2016). A stringent *ex vivo* protocol that produces synchronized differentiation of non-adherent bone marrow-derived mononuclear phagocytic precursor cells into immature, adherent macrophages in the presence of low levels of CSF-1 (12 ng/ml) then more-mature macrophages in the presence of higher levels of CSF-1 (120 ng/ml) was used in Tushinski et al. (1982). To document the CSF-1-induced expression changes during this differentiation process, we used whole-transcriptome sequencing with a focus on expression changes underpinning the development of adhesion, motility and matrix degradation. We then used these baseline mature macrophages to delineate the effect of IL-4 on gene expression and correlate those changes to increased motility and matrix degradation in IL-4-treated macrophages. Finally, we reduced expression of the adhesion proteins paxillin and leupaxin to demonstrate their overlapping and distinct roles in CSF-1-induced spreading, adhesion and matrix degradation.

RESULTS

CSF-1 drives adhesion and spreading in differentiating mononuclear phagocytes and maturing macrophages

Non-adherent bone marrow cells were treated with increasing doses of CSF-1 as described above to collect mononuclear phagocytic precursor cells (C1), immature adherent (C2) and mature adherent (C3) macrophages for transcriptome analysis (Fig. 1A). This stepped increase in CSF-1 concentration stimulated differentiation of mononuclear phagocytic precursors from non-adherent cells into immature adherent macrophages and then into mature larger, better-spread macrophages (Fig. 1B).

Gene induction patterns in CSF-1-induced macrophage differentiation and maturation

Although BMMs cultured *in vitro* do not fully represent tissue-resident macrophages, they can be used to investigate the process of macrophage differentiation. To characterize gene expression changes underpinning the process of mononuclear phagocytic cell differentiation into adherent, mature macrophages, sequential RNA-sequencing (RNA-Seq) analysis was carried out on precursor cells (C1), immature (C2) and mature (C3) BMMs from a total of nine libraries. The similarity of the biological replicates' transcript expression profiles was demonstrated by SeqMonk principal component analysis (PCA) (Fig. 1C).

The RNA-Seq data (aligned raw reads) were then analyzed by the EdgeR pipeline in SeqMonk ($P \leq 0.01$) to identify differentially expressed genes during CSF-1-induced macrophage differentiation and maturation. CSF-1 induced the upregulation of 2407 genes and downregulation of 3355 genes as precursor cells differentiated into fully mature macrophages (C1 to C3) (Fig. 1D, C3 versus C1; Table S1). Most gene expression changes occurred during the differentiation step from non-adherent to adherent cells (C1 to C2) with fewer changes occurring during subsequent maturation (C2 to C3) (Fig. 1D; Table S1). Heatmaps for the top 50 down- and upregulated genes overall and for each transition are shown (Fig. 1E,F; see also Table S2), with a full list of differentially expressed genes in Tables S3 (C1 to C3), S4 (C1 to C2) and S5 (C2 to C3). Notably, the large number of points aligned on the *x*-axis of the C1-to-C3 scatter plot depicts 1239 genes for which expression was switched off altogether during differentiation into fully mature BMMs. We compared these genes to those listed for specific mouse bone marrow-derived cell populations identified in the Mouse Cell Atlas (Han et al., 2018). Consistent with commitment to macrophage differentiation, highly expressed genes in precursor cells that were switched off during this transition included neutrophil markers calgranulin B (*S100a9*), neutrophilic granule protein (*Ngp*) and lactotransferrin (*Ltf*), B-cell markers *Cd79a* and *Cd19*, and dendritic cell markers *Flt3* and *Siglech* (Han et al., 2018) (Tables S1 and S6). The validity of our step-wise C1–C2–C3 differentiation model was supported by evidence that genes downregulated during differentiation of monocytes into colonic macrophages, such as *Ly6C* (also known as *Ly6c2*) and selectin-L (*Sell*) (Schridde et al., 2017), were all but switched off during C1-to-C2 differentiation, while expression of *Ccr2*, the receptor for the monocyte chemokine *Ccl2*, was lost in the C2-to-C3 maturation step (Tables S2-S5).

In contrast to the preponderance of hematopoietic lineage markers in the downregulated gene set, the top upregulated genes in differentiating macrophages encoded proteins with disparate functions, including structural (*Nes*, *Fat3* and *Emp2*), metabolic

Journal of Cell Science (2020) 133, jcs232405. doi:10.1242/jcs.232405

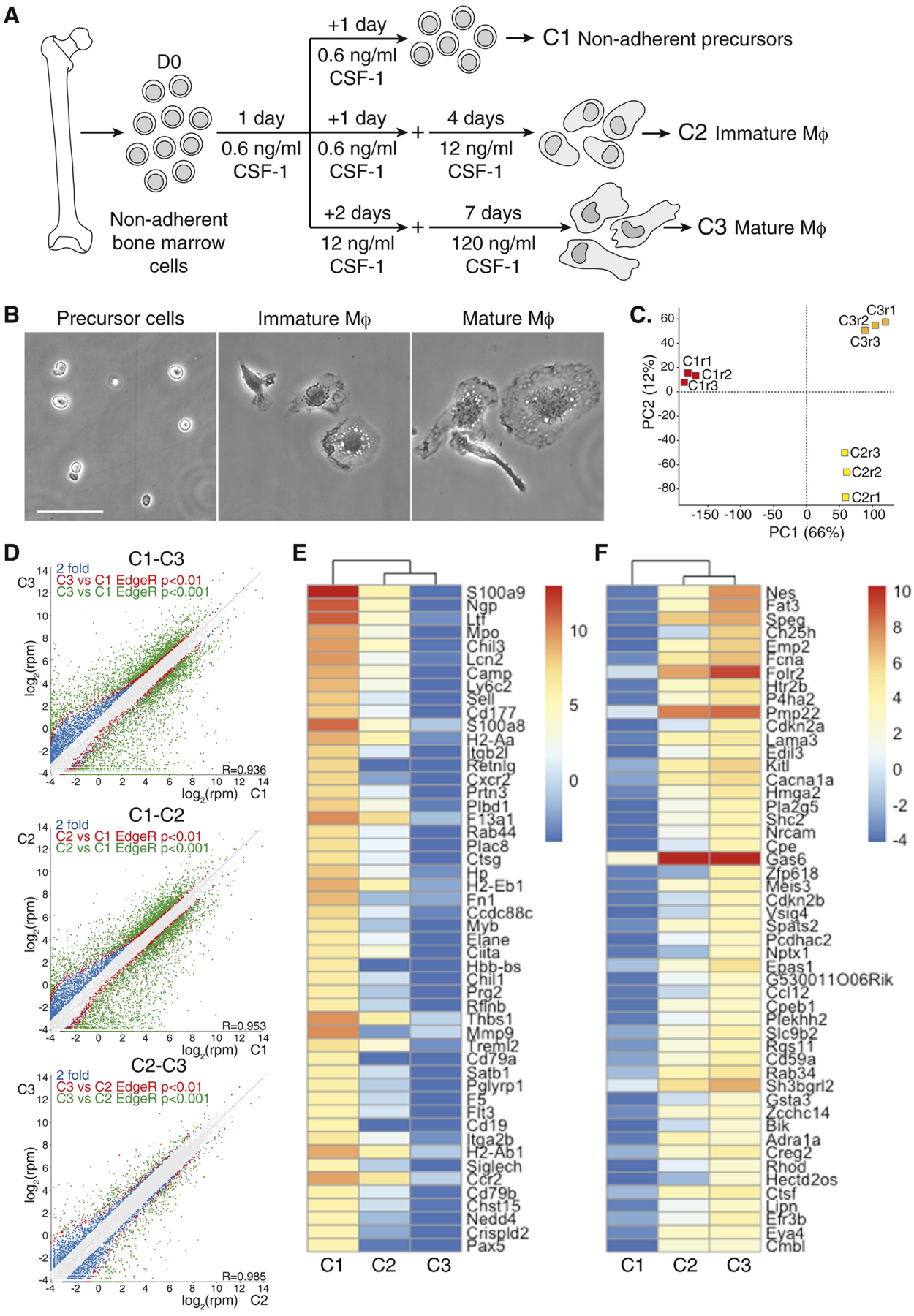

Fig. 1. See next page for legend.

Journal of Cell Science (2020) 133, jcs232405. doi:10.1242/jcs.232405

Fig. 1. Experimental outline and gene induction patterns in CSF-1-induced BMM differentiation and maturation. (A) Freshly extracted non-adherent bone marrow cells from three separate mice were grown for 1 day in 0.6 ng/ml CSF-1 then divided into three samples for either a second day of 0.6 ng/ml CSF-1 (C1), a second day of 0.6 ng/ml CSF-1 plus 4 days of 12 ng/ml CSF-1 (C2), or 2 days of 12 ng/ml and 7 days of 120 ng/ml CSF-1 (C3). (B) Representative phase-contrast images of non-adherent precursors (C1), immature macrophages (C2) and mature macrophages (C3). Scale bar: 20 µm. (C) Principal component analysis (PCA) of bulk RNA-Seq data from biological replicates (r1–r3) of non-adherent precursors, immature macrophages and mature macrophages. (D) Scatter plots of gene expression with depiction of 2-fold or more differentially expressed genes (blue) at significance level $P<0.01$ (red) and $P<0.001$ (green), as determined by the EdgeR pipeline in SeqMonk. R represents correlation co-efficient. (E,F) Heatmaps of the top 50 downregulated (E) and upregulated (F) genes during macrophage differentiation.

(*Ch25h*) and the immune response (*Fcna*). We compared our list of significantly upregulated genes with markers of four *in vivo* mouse macrophage clusters (Han et al., 2018). Of the 85 markers found in all *in vivo* macrophage clusters, 44 were strongly upregulated during *in vitro* BMM differentiation, indicating that BMMs differentiated in the presence of CSF-1 *in vitro* are very similar to tissue-resident macrophages (Table S6) (Han et al., 2018). Importantly, CSF-1-differentiated macrophages did not express significant levels of either classically activated (M1) markers *Il-6* or *Nos2*, or alternatively activated (M2) markers *Arg1*, *Chil3* and *Retnla*.

Gene ontology (GO) functional analysis shows enrichment of adhesion and motility pathways

To identify the major biological processes up- and downregulated during step-wise differentiation of bone marrow precursors into mature macrophages, functional pathway analysis was carried out using the PANTHER classification system (Mi et al., 2016). Pathways important for neutrophil function plus B- and T-cell lineage commitment and associated functions of interleukin production, antigen processing and immune response dominated the downregulated gene patterns (data not shown). Consistent with changes in adhesion and morphology during CSF-1 stimulation of macrophage differentiation, upregulated GO pathways included adhesion and cell migration (Fig. S1, C1–C3). Adhesion and motility pathways also scored highly during adhesion development (C1–C2) and further maturation (C2–C3) (Fig. S1).

Allocation of genes to functional pathways using an unsupervised analysis is impacted by the extent to which those genes have been annotated to pathways in reference databases. Incomplete annotation particularly affects cells with complex transcriptomes such as macrophages (Suzuki et al., 2009). Moreover, the highly specialized motility machinery of macrophages is regulated by selectively expressed proteins and splice variants (Pixley, 2012), many of which are not included in unsupervised functional pathway analyses. To catalogue CSF-1-induced changes correlating with increased adhesion and interstitial migration during macrophage differentiation, we undertook a supervised analysis of molecules important for adhesion, cytoskeleton remodeling and matrix degradation in macrophages.

CSF-1-induced macrophage differentiation and maturation is associated with extensive changes in the expression of adhesion genes and increased organization of adhesion, leading to increased footprint area

The integrated consensus adhesome of 258 proteins was derived from cells that form focal contacts (Horton et al., 2016). As macrophages form smaller adhesions and express a unique set of adhesion-regulating proteins (Pixley, 2012), we added additional genes to the consensus adhesome, including the myeloid-restricted SFKs *Hck* and *Fgr* (Dwyer et al., 2016). The curated list was used to identify changes in expression during macrophage differentiation and maturation. Of the 280 adhesion-related genes, 53 were upregulated and 58 downregulated, producing a change in expression ($P<0.01$) in almost 40% of the macrophage adhesome (Table S7). Looking at the integrin adhesion receptors in detail, two thirds of integrins expressed in either precursor cells or macrophages showed altered expression, seven upregulated (α integrins – α6, α8, α9 and αV; β integrins – β1, β2 and β5) and ten downregulated (α integrins – α1–4, αe, α2b and β integrins – β3, β4, β7 and β8) (Fig. 2A, Table 1). Notably, α9 integrin expression increased 25-fold, whereas integrins α1 and α2b became almost undetectable.

Many adhesion proteins are tyrosine phosphorylated during adhesion-based signaling and turnover. FAK, its homolog Pyk2 and their associated SFKs are the tyrosine kinases responsible for adhesion protein phosphorylation (Pixley, 2012; Zaidel-Bar et al., 2007). Macrophages express both FAK and Pyk2 (Owen et al., 2007), as well as five SFKs, Src, Fyn, Hck, Fgr and Lyn (Dwyer et al., 2016; Abram and Lowell, 2008). *Ptk2* (which encodes FAK) was upregulated 7-fold during CSF-1-stimulated BMM differentiation, although final levels remained almost 8-fold lower than the abundantly expressed *Pyk2* (Table 1). Of the SFKs, *Fyn* and *Hck* increased, whereas *Fgr* levels fell sharply (Table 1). The multi-adaptor adhesion protein paxillin is phosphorylated by the adhesion kinases and dephosphorylated by the tyrosine phosphatase *PTPRO* (Zaidel-Bar et al., 2007; Pixley et al., 2001). While the expression of *PTPRO* increased more than 3-fold in differentiating macrophages, paxillin expression decreased and leupaxin, a paxillin family member, increased commensurately, while vinculin and zyxin decreased markedly (Table 1).

We used structured illumination super-resolution microscopy (SIM) to document maturation changes in the small adhesion structures found in macrophages. BMMs were stimulated with CSF-1 for 10 min to maximize adhesion formation and phosphopaxillin (pY118 paxillin) was used to detect point contacts, which are difficult to discern over background staining when imaged by total paxillin or other adhesion markers (Pixley, 2012; Pixley et al., 2001). Striking changes in adhesion size and distribution were seen as macrophages matured. CSF-1 induced the formation of coarse focal complexes with few point contacts at the leading edge of immature BMMs in contrast to the tiny point contacts and linear focal complexes seen under spreading lamellipodia of mature BMMs (Fig. 2B, left column). Changes in adhesion number, type and distribution are more evident when phosphopaxillin signal intensity is converted to a binary signal (Fig. 2B, right column). Moreover, mature BMMs appeared larger than immature macrophages and this was confirmed by tracing the footprint area of BMMs, which confirmed a more than 2.5-fold increase in size as adherent macrophages mature (Fig. 2C).

Cadherins and catenins may also regulate macrophage adhesion. Similar to the cell-matrix adhesome, the cadherin adhesome undergoes significant expression changes as macrophages mature. Table S8 lists members of the large cadherin superfamily and associated catenins expressed at reliably detectable levels (>5 reads) at one or more stages during macrophage differentiation. The most striking change seen was a >2000-fold upregulation of the atypical cadherin *Fat3* (see heatmap in Fig. 1F), and several members of the protocadherin and catenin families show significant upregulation, whereas expression of E-cadherin is strongly downregulated during the development of cell-matrix adhesions (Table S8).

Journal of Cell Science (2020) 133, jcs232405. doi:10.1242/jcs.232405

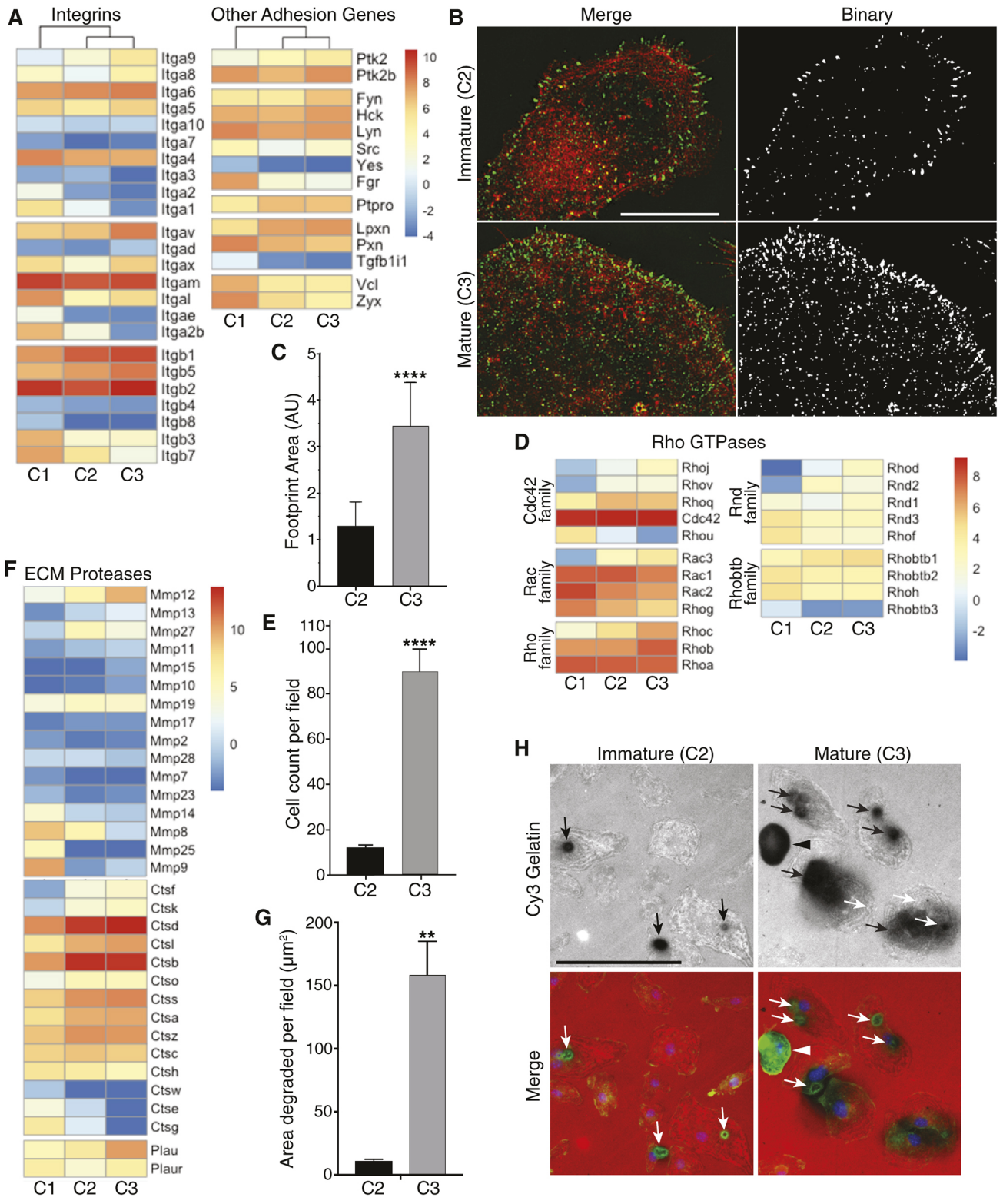

Fig. 2. See next page for legend.

CSF-1-induced macrophage differentiation is associated with extensive changes in the expression of cytoskeletal remodeling genes and an increase in cell motility

Consistent with the requirement for cytoskeletal remodeling in spreading and migration, over 80% of Rho family members showed significant expression changes during macrophage differentiation (Fig. 2D, Table 2). Upregulated molecules included *Cdc42*, *RhoJ* and *RhoV* (Cdc42 subfamily), *Rac3* (Rac subfamily), *RhoB* and *RhoC* (Rho subfamily), *RhoD* and *Rnd2* (Rnd subfamily) and *RhoBTB1* (RhoBTB subfamily). *Rac2* and *RhoG* (Rac subfamily), *RhoF* and *Rnd3* (Rnd subfamily), *RhoH, RhoBTB2* and *RhoBTB3* (RhoBTB subfamily) and *RhoU* (Cdc42 subfamily) were

Journal of Cell Science (2020) 133, jcs232405. doi:10.1242/jcs.232405

Fig. 2. CSF-1-induced BMM maturation alters the expression of adhesion, actin cytoskeletal remodeling and matrix-degrading genes and is associated with increased adhesions, footprint area, migration and matrix degradation. (A) Heatmaps of integrins and other core adhesion genes in non-adherent precursors (C1), immature BMMs (C2) and mature BMMs (C3). (B) C2 and C3 BMMs grown on fibronectin-coated coverslips were stimulated with CSF-1 for 10 min to maximize adhesion formation. Structured illumination microscopy (SIM) images of representative cells shows a spreading lamellipodium stained for pY118 paxillin (green) and F-actin (red) in the left column, with binary representations of pY118 paxillin signals in the right column. Scale bar: 10 µm. *n*=4. (C) C2 and C3 BMMs were grown in the continuous presence of CSF-1 before fixation and imaging by epifluorescent microscopy and cell tracing to measure footprint area. >50 cells were examined per experiment. *n*=3, mean±s.e.m., ****P<0.0001, Student's *t*-test. (D) A heatmap of Rho family GTPase gene expression in C1, C2 and C3 cells. (E) To assess motility, C2 and C3 BMMs were seeded in the upper chamber of transwell inserts in CSF-1-free medium, with CSF-1-containing medium (120 ng/ml) in the lower chamber. Cells migrating towards CSF-1 and adhering to the underside of the membrane were quantified. *n*=3, mean±s.e.m., ****P<0.0001, Student's *t*-test. (F) A heatmap of ECM protease gene expression in C1, C2 and C3 cells. (G) Average area of degradation per field for C2 and C3 BMMs was corrected for cell number. Five fields/sample were quantified. *n*=3, mean±s.e.m., **P<0.01, Student's *t*-test. (H) C2 and C3 BMMs were plated on Cy3-labeled gelatin (red) for 24 h before fixation and staining for F-actin (green) and nuclei (blue). Arrows indicate rosettes associated with degradation and arrowheads indicate a cell showing degradation under the entire cell outline. Scale bar: 10 µm.

downregulated. Of the Rho family GAPs and GEFs expressed in precursor cells or differentiating macrophages, 60% showed significant expression changes when mature macrophages (C3) were compared with non-adherent cells (C1) (Table S9). This increased to 70% when genes with a significant but transient change in expression during development of adhesion, such as *Arap3*, were also included.

Rho family GTPases activate many downstream effectors that act on the actin cytoskeleton and other cellular targets (Bustelo et al., 2007). We used the open access REACTOME database to identify Rho family actin cytoskeletal effectors (https://reactome.org/). Expression of more than half of the effectors changed significantly during differentiation (C1 to C3), and this increased to almost 70% when transient changes were included (Table S10). Thus, most genes regulating the actin cytoskeleton in macrophages are themselves regulated by the process of differentiation. Finally, intermediate filaments have been shown to regulate cell motility as well as maintain the mechanical integrity of cells (Cheng and Eriksson, 2017). Hence, nestin (*Nes*), which is the most highly upregulated gene during differentiation (>2600-fold, heatmap in Fig. 1F), may also influence macrophage migration (Tables S2 and S11).

The changes in adhesion number and distribution and the increase in cell size plus the changes in expression of cytoskeletal regulators suggested that migration speed increases as macrophages mature. CSF-1-stimulated chemotaxis was assessed by transwell assay, which showed a 7-fold increase in motility in mature over immature macrophages (Fig. 2E). Thus, widespread changes in the expression of adhesion and cytoskeletal regulatory molecules during macrophage maturation support a profound increase in macrophage migration speed.

CSF-1-induced macrophage maturation is associated with extensive changes in the expression of extracellular protease genes and increased matrix degradation

As interstitial migration requires degradation of matrix proteins, we looked for significant changes in the expression of members of the three ECM-digesting groups expressed in macrophages (Fig. 2F, Table 3). Over 70% of expressed extracellular proteases (23 of 32) demonstrated significant changes in expression. *Mmp12*, *Mmp13* and *Mmp27* showed significant upregulation, while several MMPs were strongly downregulated: *Mmp8*, *Mmp9* and the membrane-type MMPs, *Mmp14* (MT1-MMP) and *Mmp25* (MT6-MMP) (Fig. 2F). The cathepsin family demonstrated even more striking changes. Many cathepsins already highly expressed in non-adherent precursors demonstrated further increases during the development of adhesion and increased motility, notably cathepsins D, L, B, S, A and Z, while cathepsins F and K showed 100-fold and 30-fold increases, respectively, from very low levels in non-adherent cells (Fig. 2F). Finally, expression of the plasminogen activator *Plau* increased 27-fold (Fig. 2F, Table 3). To examine whether extracellular protease expression changes altered the capacity of maturing macrophages to degrade ECM, we compared the ability of immature adherent (C2) and mature adherent (C3) macrophages to digest Cy3-conjugated gelatin. Degradation was directly associated with actin-rich podosomal rosettes at both stages of maturation although it often extended well beyond rosette outlines in mature macrophages (Fig. 2H, arrows). Maturation produced a 5-fold increase in the rate of rosette formation and some mature macrophages formed podosomal arrays that produced degradation under the entire cell (Fig. 2H, arrowheads). Consequently, the total area digested increased 14-fold in mature macrophages (Fig. 2G). Taken together, these results indicate that CSF-1-induced differentiation produces mature macrophages that adhere and spread better, migrate faster, form more rosettes and degrade matrix more efficiently than immature macrophages.

IL-4-induced activation increases BMM migration and matrix degradation

Determination of the changes associated with CSF-1-induced macrophage differentiation allowed more-precise characterization of the effects of IL-4 activation on macrophage function and gene expression. To examine changes in morphology, mature BMMs were grown for 2 days in CSF-1±20 ng/ml IL-4. Compared to baseline BMMs, IL-4-activated BMMs were elongated and often multipolar (Fig. 3A). Cell tracing of F-actin-stained images demonstrated that IL-4 treatment doubled elongation (Fig. 3B). To quantify the multipolar changes, cells were grouped according to whether they had a single circular or leading-edge lamellipodium, or two, three or more pseudopodia. More than 50% of IL-4-treated macrophages had two or more pseudopodia compared to fewer than 20% of baseline BMMs (Fig. 3C). CSF-1-induced chemotaxis and matrix-degradation assays were then carried out and IL-4 was shown to enhance motility 3.5-fold and degradation 2-fold (Fig. 3D,E).

IL-4-induced activation alters the expression of migratory machinery molecules

To determine if IL-4-induced changes in macrophage function were underpinned by gene expression changes, the transcriptomes of baseline and IL-4-treated BMMs were analyzed. As single-base resolution was not required for this analysis, AmpliSeq was used in the identification of differentially expressed genes (Li et al., 2015). IL-4 treatment produced 750 upregulated and 699 downregulated genes (EdgeR, $P \leq 0.01$; Table S11). Consistent with previous studies, well-known markers of IL-4-induced macrophage activation, *Arg1* and *Retnla*, were amongst the most highly upregulated genes, along with *Ocstamp*, a recently recognized IL-4-induced gene (Fig. 3F, Table 4) (Martinez et al., 2013; Martinez and Gordon, 2014; Yuan et al., 2017). All three showed striking increases in expression from undetectable or low levels,

Journal of Cell Science (2020) 133, jcs232405. doi:10.1242/jcs.232405

Table 1. Core adhesion genes

Protein	Gene	C3/C1	*P*-value	C2/C1	*P*-value	C3/C2	*P*-value	Mean log2 RPM		
								C1	C2	C3
Integrin α1	*Itga1*	0.002	0.001	0.04	0.001	0.05	0.001	5.73	1.08	−3.16
Integrin α2	*Itga2*	0.022	0.001	0.05	0.001	0.48	ns	1.78	−2.67	−3.73
Integrin α3	*Itga3*	0.31	0.001	1.31	ns	0.24	ns	−2.36	−1.97	−4.05
Integrin α4	*Itga4*	0.50	0.05	0.59	ns	0.85	ns	8.12	7.36	7.13
Integrin α5	*Itga5*	0.98	ns	0.45	0.001	2.18	0.05	6.14	4.98	6.11
Integrin α6	*Itga6*	1.67	0.01	1.40	0.01	1.19	ns	7.61	8.09	8.34
Integrin α7	*Itga7*	0.56	ns	0.39	0.05	1.43	ns	−2.70	−4.07	−3.55
Integrin α8	*Itga8*	2.29	0.05	0.22	0.01	10.47	0.001	3.26	1.07	4.46
Integrin α9	*Itga9*	25.67	0.001	4.19	0.001	6.12	0.001	0.58	2.65	5.27
Integrin α10	*Itga10*	0.77	ns	0.62	0.01	1.24	ns	−0.35	−1.04	−0.72
Integrin α11	*Itga11*	1.04	ns	1.02	ns	1.02	ns	−4.10	−4.07	−4.05
Integrin αD	*Itgad*	2.59	ns	0.72	ns	3.61	ns	−2.69	−3.17	−1.32
Integrin αE	*Itgae*	0.029	0.001	0.03	0.001	0.94	ns	1.82	−3.17	−3.26
Integrin αIIb	*Itga2b*	0.001	0.001	0.04	0.001	0.03	0.001	6.80	2.15	−2.99
Integrin αL	*Itgal*	0.24	0.01	0.06	0.001	3.87	0.001	7.85	3.87	5.82
Integrin αM	*Itgam*	0.79	ns	0.62	ns	1.27	ns	9.84	9.14	9.49
Integrin αV	*Itgav*	4.15	0.001	1.25	ns	3.33	0.001	6.23	6.55	8.28
Integrin αX	*Itgax*	1.37	ns	0.11	0.001	12.73	0.001	5.80	2.59	6.26
Integrin β1	*Itgb1*	3.47	0.001	2.66	0.001	1.31	ns	7.67	9.08	9.46
Integrin β2	*Itgb2*	1.40	0.01	0.57	ns	2.45	0.001	10.11	9.30	10.59
Integrin β3	*Itgb3*	0.06	0.001	0.05	0.001	1.23	ns	7.00	2.73	3.02
Integrin β4	*Itgb4*	0.48	0.01	0.58	0.05	0.82	ns	−1.92	−2.70	−2.99
Integrin β5	*Itgb5*	2.96	0.001	1.66	0.001	1.78	0.05	6.90	7.64	8.47
Integrin β6	*Itgb6*	1.00	ns	0.99	ns	1.02	ns	−4.05	−4.07	−4.05
Integrin β7	*Itgb7*	0.02	0.001	0.22	0.001	0.09	0.001	7.48	5.32	1.92
Integrin β8	*Itgb8*	0.17	0.001	0.16	0.001	1.02	ns	−1.45	−4.07	−4.05
FAK	*Ptk2*	7.10	0.001	3.44	0.001	2.06	ns	2.14	3.93	4.97
Pyk2	*Ptk2b*	1.14	ns	0.56	0.05	2.01	0.01	7.73	6.91	7.92
Src	*Src*	0.43	ns	0.17	0.001	2.57	ns	4.09	1.50	2.86
Fyn	*Fyn*	2.58	0.001	0.84	ns	3.08	0.001	5.15	4.90	6.52
Yes	*Yes*	0.21	0.001	0.27	0.001	0.76	ns	−1.77	−3.64	−4.05
Hck	*Hck*	1.42	0.05	0.86	ns	1.64	ns	7.12	6.91	7.63
Fgr	*Fgr*	0.02	0.001	0.03	0.001	0.56	ns	7.54	2.55	1.71
Lyn	*Lyn*	0.73	ns	0.59	0.05	1.23	ns	8.19	7.44	7.73
PTPRO	*Ptpro*	2.98	0.001	3.34	0.001	0.89	ns	4.98	6.73	6.56
Paxillin	*Pxn*	0.30	0.001	0.46	0.001	0.65	ns	8.13	7.00	6.38
Hic-5	*Tgfb1i1*	0.05	0.001	0.07	0.001	0.71	ns	0.75	−3.06	−3.55
Leupaxin	*Lpxn*	4.47	0.001	3.46	0.001	1.29	ns	5.64	7.43	7.80
Vinculin	*Vcl*	0.19	0.001	0.22	0.001	0.89	ns	7.20	5.00	4.84
Zyxin	*Zyx*	0.08	0.001	0.21	0.001	0.39	ns	8.05	5.80	4.46

C1, non-adherent precursor cells; C2, immature adherent macrophages; C3, mature adherent macrophages; ns, not significant; RPM, reads per million reads.

supporting the notion that CSF-1 produces baseline (M0) macrophages *in vitro* (Murray et al., 2014). *Chil3* was not included in the AmpliSeq 20,000 mouse gene expression primer set, but the expression of two recently identified 'M2' markers, *Egr2* and *Tgm2*, was also increased (28-fold and 2.3-fold, respectively; Table S12) (Jablonski et al., 2015; Martinez et al., 2013).

As IL-4-activated macrophages migrate and degrade matrix more efficiently than baseline macrophages, we examined whether IL-4 treatment alters the expression of genes regulating the motility machinery. The most striking change in core adhesion molecules was the 100-fold upregulation of integrin αX, with a 2.3-fold increase in expression of its partner β2 integrin (Fig. 3F, Table 4; Tables S12 and S13). Integrins α5, β3, β7 and β8 were also upregulated, whereas expression of integrins α6, α8 and α9 decreased (Table S12). Phosphotyrosine regulators of adhesion were affected, with upregulation of *Ptk2* (which encodes FAK), *Src* and *Fyn*, downregulation of *Hck*, *Lyn* and *Ptpro*, and leupaxin becoming more abundant than paxillin (Table S12). Associated with the adhesion changes was a 120-fold upregulation of the ECM protein fibronectin (Fig. 3F). Several Rho family GTPases also showed significant changes in expression, with increases in *RhoB* (3-fold), *RhoC* (4-fold), *RhoH* and *RhoJ* (2-fold each), and *RhoV* (15-fold), and marked downregulation of *Rac3*, *RhoD* and *RhoF* (Table S12). Expression of the intermediate filament nestin increased further, and several MMPs demonstrated striking increases in expression, particularly *Mmp12* (55-fold), *Mmp13* (110-fold) and *Mmp19* (10-fold), as did cathepsin K (9-fold) (Table S12). Thus, as for CSF-1-induced macrophage differentiation, the increased motility and matrix degradation of IL-4-activated macrophages is supported by widespread changes in the expression of genes regulating adhesion, migration and matrix degradation.

Leupaxin and paxillin contribute to macrophage spreading, adhesion numbers and matrix degradation in a non-redundant manner

Our RNA-Seq data showed a 4.5-fold increase in leupaxin expression, while paxillin decreased by 70% as macrophages developed adhesion (Table 1). SIM was used to compare the relative distributions of paxillin and leupaxin in macrophage adhesions in mature BMMs. Both proteins were found in point contacts and focal complexes, but paxillin stained more strongly than leupaxin in point contacts. Interestingly, leupaxin and paxillin localization did not overlap

Journal of Cell Science (2020) 133, jcs232405. doi:10.1242/jcs.232405

Table 2. Rho family GTPases

								Mean log2 RPM		
Protein	Gene	C3/C1	*P*-value	C2/C1	*P*-value	C3/C2	*P*-value	C1	C2	C3
Cdc42	*Cdc42*	1.28	0.05	1.30	0.05	0.99	ns	8.84	9.22	9.20
Rac1	*Rac1*	0.59	ns	1.03	ns	0.57	ns	7.89	7.94	7.14
Rac2	*Rac2*	0.25	0.001	0.41	0.001	0.61	ns	8.38	7.09	6.36
Rac3	*Rac3*	90.03	0.001	31.14	0.001	2.89	0.01	−2.16	2.81	4.34
RhoA	*Rhoa*	0.87	ns	0.92	ns	0.95	ns	7.96	7.85	7.77
RhoB	*Rhob*	2.33	0.001	1.01	ns	2.31	0.001	6.60	6.62	7.82
RhoC	*Rhoc*	20.57	0.001	6.70	0.001	3.07	0.001	2.06	4.80	6.42
RhoD	*Rhod*	102.38	0.001	22.01	0.001	4.65	0.001	−3.96	0.50	2.71
RhoF/Rif	*Rhof*	0.19	0.001	0.23	0.001	0.83	ns	4.56	2.46	2.19
RhoG	*Rhog*	0.23	0.001	0.44	0.01	0.52	ns	7.16	5.97	5.02
RhoH	*Rhoh*	0.37	0.05	0.33	0.001	1.13	ns	4.84	3.23	3.41
RhoJ/Tc10L	*Rhoj*	22.06	0.001	5.85	ns	3.77	0.01	−1.61	0.93	2.85
RhoQ/Tc10A	*Rhoq*	3.34	0.001	3.82	0.001	0.87	ns	3.89	5.83	5.63
RhoU/Wrch1	*Rhou*	0.01	0.001	0.05	0.001	0.13	ns	4.59	0.17	−2.76
RhoV/Wrch2	*Rhov*	17.88	0.001	14.56	0.001	1.23	ns	−2.35	1.52	1.81
RhoBTB1	*Rhobtb1*	3.18	0.001	2.39	0.001	1.33	ns	3.23	4.48	4.90
RhoBTB2	*Rhobtb2*	0.51	0.01	0.56	0.01	0.90	ns	4.50	3.67	3.52
RhoBTB3	*Rhobtb3*	0.17	0.001	0.15	0.001	1.09	ns	−0.21	−2.93	−2.81
Rnd1	*Rnd1*	1.47	ns	0.47	0.001	3.11	0.01	2.00	0.92	2.55
Rnd2	*Rnd2*	19.72	0.001	46.09	0.001	0.43	ns	−2.67	2.86	1.63
Rnd3	*Rnd3*	0.36	0.001	0.33	0.001	1.12	ns	4.55	2.93	3.09

C1, precursor cells; C2, immature adherent macrophages; C3, mature adherent macrophages; ns, not significant; RPM, reads per million reads.

precisely in focal complexes (Fig. 4A, inset). Adhesion numbers were quantified by binary analysis and showed a 1.4-fold greater number of paxillin-rich adhesions compared with leupaxin (Fig. 4B,C).

These differences led us to examine whether paxillin and leupaxin have similar or distinct functions. Significant biological effects were seen, with a 40% and 60% reduction in paxillin and

Table 3. ECM proteases

								Mean log2 RPM		
Protein	Gene	C3/C1	*P*-value	C2/C1	*P*-value	C3/C2	*P*-value	C1	C2	C3
MMP2	*Mmp2*	0.69	ns	0.55	ns	1.26	ns	−2.76	−3.63	−3.30
MMP7	*Mmp7*	0.39	0.01	0.39	0.01	1.01	ns	−2.70	−4.07	−4.05
MMP8	*Mmp8*	0.00	0.001	0.15	0.001	0.02	0.001	8.81	6.05	0.30
MMP9	*Mmp9*	0.00	0.001	0.00	0.001	5.39	ns	9.96	−2.64	−0.21
MMP10	*Mmp10*	3.23	ns	1.38	ns	2.33	ns	−4.10	−3.63	−2.41
MMP11	*Mmp11*	4.55	ns	2.54	ns	1.79	ns	−2.51	−1.16	−0.32
MMP12	*Mmp12*	94.07	0.001	10.03	0.001	9.38	0.001	2.71	6.03	9.26
MMP13	*Mmp13*	22.00	0.001	7.21	ns	3.05	0.05	−2.87	−0.02	1.59
MMP14	*Mmp14*	0.04	0.001	0.06	0.001	0.65	ns	4.12	−0.03	−0.66
MMP15	*Mmp15*	3.84	ns	0.99	ns	3.89	ns	−4.05	−4.07	−2.11
MMP17	*Mmp17*	1.49	ns	1.49	ns	1.00	ns	−3.43	−2.85	−2.85
MMP19	*Mmp19*	1.96	ns	2.61	0.001	0.75	ns	3.56	4.94	4.53
MMP23	*Mmp23*	0.37	ns	0.26	0.001	1.40	ns	−1.54	−3.47	−2.99
MMP25	*Mmp25*	0.00	0.001	0.00	0.001	1.02	ns	5.38	−4.07	−4.05
MMP27	*Mmp27*	12.53	0.001	55.55	0.001	0.23	0.001	−0.20	5.60	3.45
MMP28	*Mmp28*	0.44	0.001	1.06	ns	0.41	ns	0.11	0.20	−1.07
Cathepsin A	*Ctsa*	4.05	0.001	3.57	0.001	1.13	ns	7.72	9.56	9.74
Cathepsin B	*Ctsb*	7.38	0.001	8.40	0.001	0.88	ns	10.27	13.34	13.16
Cathepsin C	*Ctsc*	1.10	ns	1.45	ns	0.76	ns	8.26	8.79	8.39
Cathepsin D	*Ctsd*	8.51	0.001	4.80	0.001	1.77	ns	10.62	12.88	13.71
Cathepsin E	*Ctse*	0.00	0.001	0.10	0.001	0.05	0.001	3.62	0.23	−4.05
Cathepsin F	*Ctsf*	100.77	0.001	53.57	0.001	1.88	ns	−2.06	3.69	4.60
Cathepsin G	*Ctsg*	0.00	0.001	0.02	0.001	0.02	0.001	7.11	1.39	−4.05
Cathepsin H	*Ctsh*	0.26	0.001	0.63	ns	0.41	0.01	7.47	6.79	5.50
Cathepsin K	*Ctsk*	30.35	0.001	17.54	0.001	1.73	ns	−0.09	4.04	4.84
Cathepsin L	*Ctsl*	7.43	0.001	5.17	0.001	1.44	ns	7.17	9.54	10.07
Cathepsin O	*Ctso*	4.93	0.001	5.46	0.001	0.90	ns	3.11	5.56	5.41
Cathepsin S	*Ctss*	4.83	0.001	3.78	0.001	1.28	ns	8.47	10.39	10.74
Cathepsin W	*Ctsw*	0.11	0.001	0.10	0.001	1.02	ns	−0.81	−4.07	−4.05
Cathepsin Z	*Ctsz*	2.76	0.001	3.07	0.001	0.90	ns	8.73	10.35	10.19
uPA	*Plau*	27.38	0.001	3.24	0.001	8.45	0.001	5.34	7.04	10.12
uPAR	*Plaur*	0.94	ns	0.18	0.001	5.16	0.001	6.60	4.15	6.51

C1, precursor cells; C2, immature adherent macrophages; C3, mature adherent macrophages; ns, not significant; RPM, reads per million reads.

Journal of Cell Science (2020) 133, jcs232405. doi:10.1242/jcs.232405

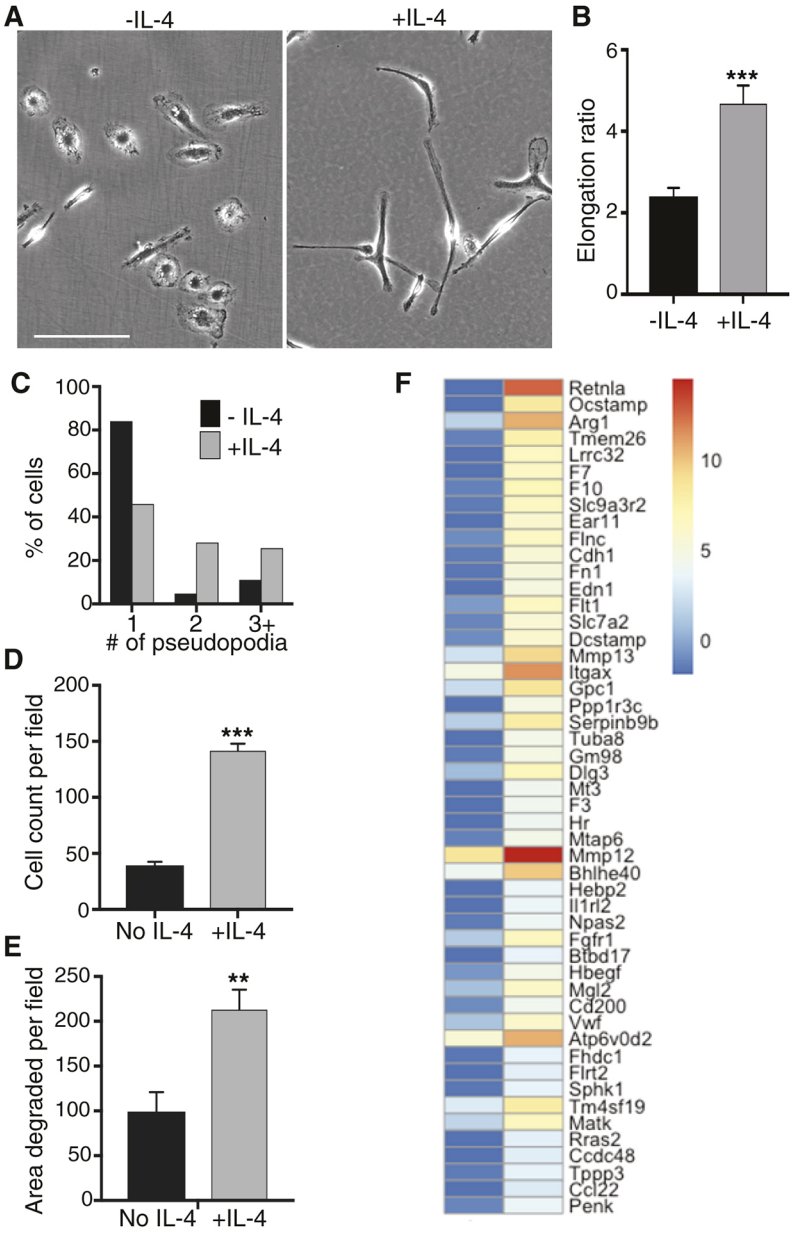

Fig. 3. IL4-induced activation alters BMM morphology and increases migration and matrix-degradative capacity. (A–C) BMMs were grown in CSF-1 (120 ng/ml) with or without 20 ng/ml IL-4 for 2 days on tissue culture dishes (A) or fibronectin-coated coverslips (B,C) before fixation. (A) Scale bar: 50 µm. (B) Fixed cells were stained for F-actin to measure elongation ratio (maximum length/maximum width). >30 cells per experiment, n=3, mean±s.e.m., ***P<0.001, Student's t-test. (C) The number of pseudopodia for each cell in B was designated as 1 if circular or a single pseudopodium, 2 if bipolar, or 3+ if three or more pseudopodia. (D) Transwell migration to CSF-1 of BMMs treated with or without IL-4 was measured. n=3, mean ±s.e.m., ***P<0.001, Student's t-test. (E) Matrix-degradative capacity of BMMs treated with or without IL-4 was measured, with five fields/sample quantified. n=3, mean±s.e.m., **P<0.01, Student's t-test. (F) A heatmap of the top 50 genes upregulated by IL-4 activation of baseline macrophages.

leupaxin, respectively, using targeted small interfering RNA (siRNA) (Fig. 4D). As demonstrated previously, CSF-1-stimulated spreading produced a 2.1-fold increase in the footprint area of control macrophages (Fig. 4E) (Sampaio et al., 2011). Spreading was attenuated 1.4-fold and 1.6-fold, respectively, when expression of either paxillin or leupaxin was reduced (Fig. 4E). Phosphopaxillin-rich adhesions were visualized by SIM to determine whether the blunted spreading responses were associated with reduced adhesion. Despite reduced total paxillin in paxillin siRNA cells, phosphopaxillin remains the clearest marker of CSF-1-stimulated macrophage point contacts. Consistent with Fig. 2B, control BMMs formed numerous point contacts right to the edge of the lamellipodium (Fig. 4F). In contrast, adhesions in paxillin siRNA cells were disorganized and their density did not increase towards the lamellipodial edge, while in leupaxin siRNA cells, elongated focal complexes anchoring thick F-actin cables formed away from the lamellipodial edge (Fig. 4F and insets). Binary image quantification confirmed a significant reduction in adhesion numbers in paxillin siRNA BMMs with a further decrease in leupaxin siRNA BMMs (Fig. 4G). As the restricted numbers of transduced cells precluded transwell motility analysis, we examined the effect of a reduction in paxillin and leupaxin expression on the ability of macrophages to degrade ECM. In contrast to their effects on the formation of adhesions, paxillin knockdown reduced matrix degradation by 66%, while a reduction in leupaxin expression did not significantly affect matrix-degrading capacity (Fig. 4H).

Thus, paxillin and leupaxin both mediate CSF-1-induced spreading and adhesion but they have distinct, non-redundant functions in the formation of adhesions and in matrix degradation.

DISCUSSION

Here, we have mapped changes in gene expression occurring during differentiation of bone marrow-derived mononuclear precursors into mature BMMs under the stimulus of the primary macrophage growth and differentiation factor, CSF-1. Although cultured macrophages do not fully represent tissue-resident macrophages

Journal of Cell Science (2020) 133, jcs232405. doi:10.1242/jcs.232405

Table 4. IL-4 top 20 differentially expressed genes

		Mean log2 RPM				Mean log2 RPM	
Up	Fold change	−IL-4	+IL-4	Down	Fold change	−IL-4	+IL-4
Retnla	22,387.8	−1.93	12.52	*Ms4a6b*	0.009	5.20	−1.61
Ocstamp	1243.8	−1.93	8.35	*Cxcl10*	0.023	4.80	−0.64
Arg1	568.0	1.54	10.69	*Fads2*	0.029	4.17	−0.96
Tmem26	503.5	−1.31	7.66	*P2ry13*	0.031	4.86	−0.14
Lrrc32	354.0	−1.93	6.53	*Siglece*	0.031	3.44	−1.56
F7	329.8	−1.93	6.43	*Cmah*	0.032	3.03	−1.94
F10	327.5	−1.40	6.96	*Itga8*	0.037	5.59	0.85
Slc9a3r2	269.6	−1.58	6.49	*Trim30c*	0.038	2.86	−1.85
Ear11	210.7	−1.93	5.78	*Oas2*	0.040	6.39	1.74
Flnc	160.9	−1.02	6.31	*Tmem176b*	0.043	3.26	−1.30
Cdh1	131.9	−1.54	5.51	*Marco*	0.045	7.91	3.42
Fn1	127.6	−1.76	5.24	*Marcksl1*	0.047	7.23	2.80
Edn1	125.4	−1.93	5.04	*Nid2*	0.048	5.11	0.72
Flt1	124.8	−0.52	6.45	*Kcnj10*	0.049	3.56	−0.79
Slc7a2	118.7	−1.20	5.69	*P2ry12*	0.050	5.80	1.47
Dcstamp	116.1	−1.00	5.86	*Afap1l1*	0.050	2.92	−1.40
Mmp13	113.8	2.44	9.27	*Gpr84*	0.054	5.09	0.89
Itgax	104.5	4.68	11.39	*Clec4e*	0.054	6.65	2.45
Gpc1	98.9	2.08	8.71	*Ifit1*	0.055	4.87	0.68
Ppp1r3c	98.0	−1.93	4.68	*Gbp9*	0.057	2.47	−1.67

RPM, reads per million reads.

in vivo, they are useful for the interrogation of cytokine-driven pathways important for macrophage differentiation and activation. To provide insights into progressive CSF-1-induced changes in gene expression, differentiating macrophages were examined in two stages: (1) initial acquisition of adhesion, and (2) subsequent maturation of adhesive, migration and matrix-degrading capabilities in adherent cells. As expected, scatter plots of gene expression demonstrated that immature and mature adherent BMMs were more closely related to each other than they were to non-adherent mononuclear phagocytic precursor cells. This was reflected in the 5.5-fold fewer differentially expressed genes in the C2-to-C3 transition than in the C1-to-C2 transition (Fig. 1). Nevertheless, as the significant downregulation of the monocyte chemokine receptor *Ccr2* in the C2-to-C3 transition shows, important expression changes continue as macrophages mature. Neutrophil, B-cell and dendritic cell markers were strongly downregulated, as were the *Myb*, *E2f2–4* and *Nfyb,c* transcription factors. The transcription factors were also switched off during phorbol ester-induced differentiation of THP-1 monocytic leukemia cells into adherent, mature macrophage-like cells (Suzuki et al., 2009) (Table S3).

Consistent with the development of an adherent phenotype upon exposure to increasing doses of CSF-1, the top upregulated pathways regulated cell adhesion and motility. Biological assays confirmed increased adhesion, motility and matrix-degrading capacity in maturing macrophages. To further validate our findings, we compared our upregulated genes to those characterizing the four macrophage populations found in the mouse by single-cell RNA-Seq (Han et al., 2018). More than 50% of the markers found in all four *in vivo* populations were upregulated and abundantly expressed in CSF-1-differentiated BMMs. Importantly, our *in vitro*-differentiated macrophages do not express significant levels of the 'M2' markers *Arg1*, *Chil3* or *Retnla*, indicating that CSF-1-differentiated macrophages are baseline or resting BMMs that can be used to examine the effects of activating cytokines such as IL-4 (Murray et al., 2014).

Since curated GO gene lists likely do not include several of these important motility machinery molecules, a supervised analysis of adhesion, actin regulatory and matrix-degrading molecules was undertaken. Non-adherent, monocyte-like precursor cells and adherent macrophages express all four members of the leukocyte-restricted β2 integrin (Cd18) family: αL(Cd11a)β2, αM(Cd11b)β2, αX(Cd11c)β2 and αD(Cd11d)β2, with abundant expression of αMβ2 integrin (Mac-1) that increases further as macrophages mature (Table 1). In contrast, αL integrin significantly decreases during differentiation, suggesting that Cd11a and Cd11b may play different roles in diapedesis and interstitial migration. Both αMβ2 and αLβ2 integrins have been reported to assist monocyte transmigration (Weerasinghe et al., 1998). β1 integrin is also strongly upregulated during differentiation along with a 25-fold upregulation of one of its partners, α9 integrin. α9β1 integrin is highly homologous to the abundantly expressed α4β1 integrin and both bind the ECM protein osteopontin to regulate macrophage motility (Lund et al., 2013). β1 integrin also mediates adhesion to additional ECM proteins, fibronectin (FN) and laminin (LN) with its highly expressed partners, α5 and α7 integrins.

Expression of FAK, Hck and PTPRO, which regulate adhesion protein phosphorylation, is also increased during differentiation and this is reflected in the marked increase in number and degree of organization of phosphopaxillin-rich adhesions (Fig. 2). Unexpectedly, however, expression of the core adhesion molecule, paxillin, decreased, while that of its selectively expressed family member, leupaxin, increased. The paxillin family of multi-adaptor adhesion proteins consists of the ubiquitously expressed paxillin, the hematopoietically enriched leupaxin and Hic-5, which was not detected in adherent BMMs (Deakin et al., 2012). Although leupaxin was first identified in macrophages (Lipsky et al., 1998), very little is known about its role in these cells. We used super-resolution microscopy to show that, like paxillin, leupaxin is found in macrophage adhesions. However, while paxillin is evenly distributed across focal complexes and point contacts, leupaxin strongly localizes to focal complexes. Moreover, the two adhesion proteins do not precisely colocalize within focal complexes. It is interesting that leupaxin is upregulated during the transition from a focal complex-based adhesion pattern in C2 BMMs to a point contact-based spreading mechanism in C3 BMMs. Consistent with this, lamellipodia of leupaxin knockdown BMMs

Journal of Cell Science (2020) 133, jcs232405. doi:10.1242/jcs.232405

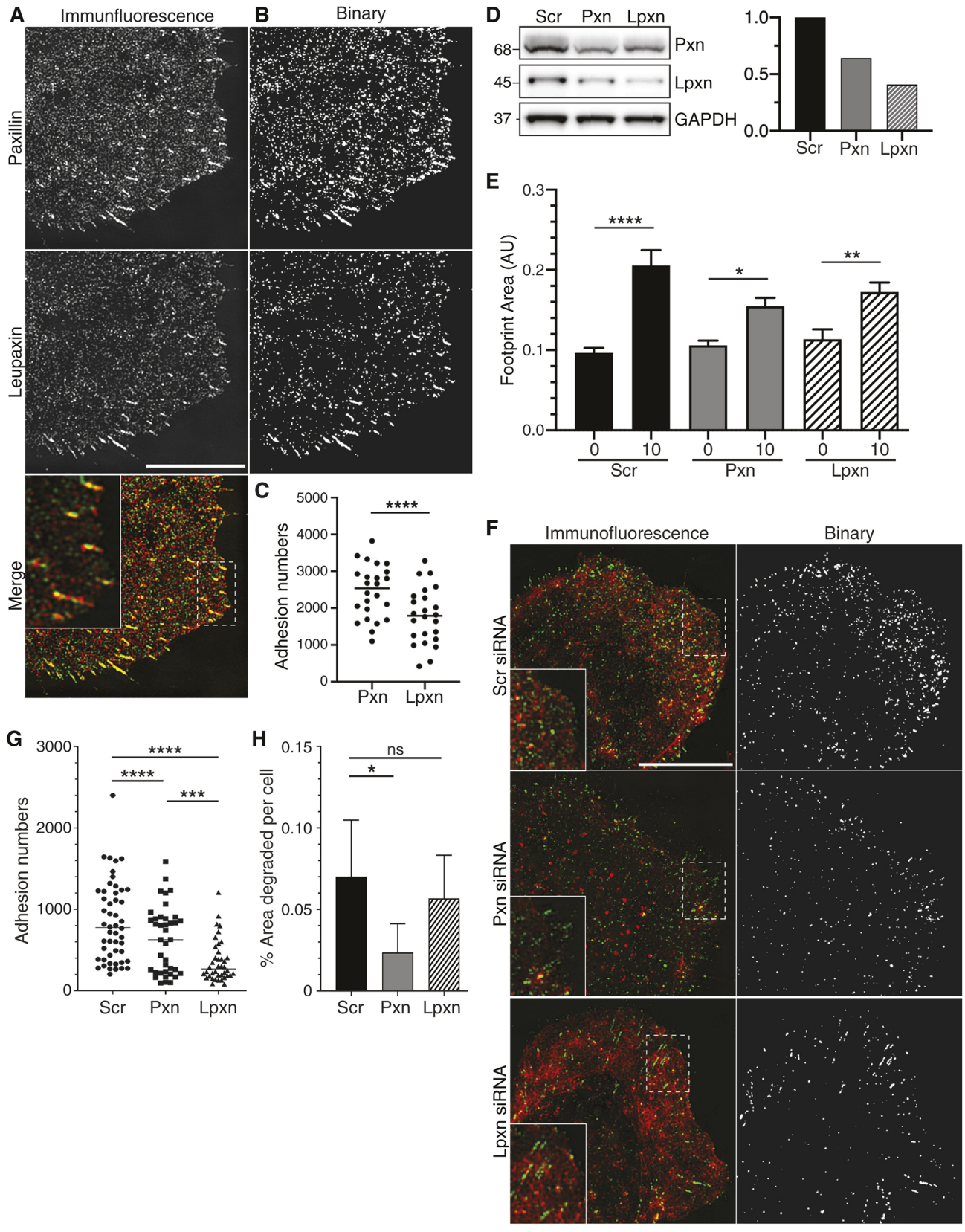

Fig. 4. See next page for legend.

contain elongated focal complexes with very few point contacts, leading to a striking overall reduction in adhesion numbers (Fig. 4). In contrast, lamellipodia of paxillin siRNA BMMs contain a disorganized mix of point contacts and focal complexes, with a less marked decrease in adhesion numbers than leupaxin siRNA BMMs. Nevertheless, the CSF-1-induced spreading responses of BMMs with

Journal of Cell Science (2020) 133, jcs232405. doi:10.1242/jcs.232405

Fig. 4. Paxillin or leupaxin have overlapping and distinct roles in macrophage adhesion, spreading and matrix degradation. (A) SIM of a typical leading lamellipodium in a CSF-1-stimulated mature BMM stained for paxillin (red in merge) and leupaxin (green in merge). The dashed line box indicates the area represented in the inset. Scale bar: 10 µm. *n*=3. (B) Binary images of adhesions stained for paxillin (top) or leupaxin (bottom). (C) Quantification of the number of adhesions containing leupaxin or paxillin in leading lamellipodia. *n*=3, mean±s.e.m., ****P<0.0001, Student's *t*-test. (D) A representative western blot of lysates from BMMs transfected with siRNA for scrambled (*Scr*, 1.0 µM), paxillin (*Pxn*, 0.8 µM) and leupaxin (*Lpxn*, 1.0 µM) sequences. Plot shows densitometric ratios of paxillin and leupaxin against GAPDH. (E) Quantification of siRNA-treated F-actin-stained cell footprint areas after CSF-1 stimulation for 0 or 10 min. >50 cells per condition, *n*=4, mean±s.e.m., *P<0.05, **P<0.01, ****P<0.0001, two-way ANOVA. (F) SIM of representative siRNA-treated CSF-1-stimulated BMMs fixed and stained for pY118 paxillin (green) and F-actin (red) (left column), with binary images of pY118 paxillin staining, thresholded for background (right column). The dashed line boxes indicate the areas shown in the insets. Scale bar: 10 µm. *n*=3. (G) Quantification of numbers of pY118 paxillin-rich adhesions under leading lamellipodia of siRNA-treated CSF-1-stimulated BMMs. *n*=3, mean ±s.e.m., ***P<0.001, ****P<0.0001, one-way ANOVA. (H) Percentage area degraded per cell was calculated for siRNA-treated BMMs cultured in CSF-1 and IL-4. Five fields per condition, *n*=3, mean±s.e.m., *P<0.05, two-way ANOVA; ns, not significant.

reduced paxillin or leupaxin expression are similarly blunted, whereas the matrix-degrading capacity of macrophages was reduced with paxillin but not leupaxin siRNA. It seems that a finely tuned balance of leupaxin and paxillin is required for mature macrophages to assemble their distinctive mix of point contacts and focal complexes under spreading lamellipodia, while paxillin may play a bigger role in matrix degradation. Interestingly, a recent study in RAW264.7 macrophages, which are not CSF-1-dependent, demonstrated that leupaxin recruitment into podosomes regulated paxillin phosphorylation and podosome turnover (Klapproth et al., 2019).

Little is known about the role of cadherins and catenins in macrophage adhesion. Macrophages have been shown to express E-cadherin (Van den Bossche et al., 2012), but we show that its expression drops sharply in adherent BMMs, whereas several protocadherin and catenin molecules increase. The most striking of these is the 2000-fold increased expression of *Fat3* (Fig. 1F). Fat-like cadherins have been shown to facilitate migration in many cell types (Horne-Badovinac, 2017), with Fat3 specifically shown to regulate directed migration of amacrine neurons in the developing retina by interacting with Ena/VASP proteins at the leading edge (Krol et al., 2016). Since macrophages and neurons share selective expression of several molecules in the motility machinery and are the only cell types demonstrated to form point contacts (Pixley, 2012), Fat3 may regulate migration similarly in macrophages as in amacrine neurons.

Actin cytoskeletal remodeling is a central element of cell motility and the Rho family of GTPases are core regulators of this process. All 21 are expressed in macrophages or their precursors and significant expression changes during macrophage differentiation were seen in the vast majority (Table 2). In macrophages, classical Rac proteins promote ruffling, lamellipodia formation and adhesion, Cdc42 stimulates filopodia formation and adhesion, and RhoA promotes acto-myosin contractility (Allen et al., 1997). However, it is difficult to determine the overall effect of changes in expression of the various Rho GTPases as the final expression levels of even some of the most highly upregulated genes, such as *Rac3* (90-fold), *RhoD* (100-fold) and *RhoJ* (22-fold), remain quite low. Nevertheless, changes to ∼70% of Rho family GTPase activators, inhibitors and effectors indicate that regulation of actin cytoskeletal remodeling undergoes profound changes as macrophages become adherent and motile.

Intermediate filaments (IFs) not only maintain the structural integrity of cells but also modulate cell motility. Tissue repair transiently changes IF expression from networks that provide stability to those that permit remodeling (Cheng and Eriksson, 2017). Vimentin, which is abundant in macrophages and non-adherent precursor cells, is upregulated in injured tissues, where it enhances cell migration, possibly through mechanosensing (Cheng and Eriksson, 2017) (Table S11). Nestin, which is upregulated 2600-fold in differentiating macrophages, has previously been shown in microglia and possibly macrophages after brain injury and inflammation (Krishnasamy et al., 2017). It is also highly expressed in neural progenitor cells (Hyder et al., 2014). Indeed, the similar expression pattern of unusual motility molecules such as Fat3, Rac3 and nestin in macrophages and migrating neural progenitors, along with other molecules such as Pyk2, suggests that these two cell types share a similar mechanistic regulation of cell motility.

Depending on the density and organization of the ECM proteins, macrophages can adopt either mesenchymal or ameboid mechanisms of migration (Guiet et al., 2011; Friedl and Wolf, 2010; Linder and Wiesner, 2015). Mesenchymal motility requires the ability to secrete matrix-degrading proteases (Guiet et al., 2011). Basement membranes contain type IV collagen, LN and FN, while the main components of interstitial ECM are fibrous proteins such as type I and III collagens, elastin, FN and tenascin plus the proteoglycans perlecan and aggrecan (Frantz et al., 2010; Hynes and Naba, 2012). Thus, it is likely that monocytes migrating through the endothelial basement membrane use different ECM proteases to macrophages migrating through interstitial tissue. These differences are reflected in the extensive and highly significant expression changes seen for MMPs, cathepsins and uPa (Fig. 2F, Table 3). The most strongly upregulated MMP was the macrophage elastase *Mmp12* (94-fold). *Mmp13*, which encodes a protein that cleaves interstitial collagens, and *Mmp27* were also highly upregulated although their final levels remained low in mature BMMs. Although downregulation of the neutrophil proteases *Mmp8*, *Mmp9* and *Mmp25* was expected, downregulation of *Mmp14* (MT1-MMP) was surprising, considering that others have shown it to be important in monocyte and macrophage migration (Vérollet et al., 2011). However, the divergent expression pattern of MMPs in human and mouse macrophages prevents inter-species expression profile comparisons (Newby, 2016). The cathepsins demonstrated profound changes in expression of all but one of those expressed in macrophages. Cathepsins A, B, D, L, S and Z, all of which were already expressed at levels between 140 reads per million reads (RPM) and 1500 RPM in non-adherent precursors, underwent additional increases, while cathepsin F and cathepsin K levels increased 100-fold and 30-fold, respectively, albeit from a low baseline (Fig. 2F). In contrast, expression of cathepsins E, G and W was all but switched off, and cathepsin H expression underwent a 4-fold decrease, leaving only cathepsin C unchanged. It is likely that cathepsins, along with MMP12 and uPa, play a central role in the 14-fold increase in the matrix-degrading capacity of mature macrophages. Interestingly, migration by macrophages into gelled collagen is independent of MMPs and relies on cathepsins (Van Goethem et al., 2010), whereas infiltration into tumor spheroids requires MMPs (Guiet et al., 2011). Thus, macrophages modulate expression of both groups of matrix proteases to respond to the various demands of the microenvironment.

The combined alterations in expression of adhesion, motility and matrix-degrading molecules mapped by RNA-Seq underpin development of the highly efficient migratory machinery in macrophages. By characterizing CSF-1-induced changes in

Journal of Cell Science (2020) 133, jcs232405. doi:10.1242/jcs.232405

mature macrophages, we were then able to clearly distinguish additional changes induced by IL-4. IL-4 is found in the tumor microenvironment, where it induces M2-like TAMs that co-migrate with tumor cells to promote invasion (Wyckoff et al., 2004, 2007). Hence, we focused on the effects of IL-4 on the migration machinery of macrophages. IL-4 altered morphology and increased motility in mature macrophages, which was consistent with previous studies demonstrating elongation (McWhorter et al., 2013) and increased motility (Vogel et al., 2014) in mouse and human macrophages, respectively, and increased microglial migration speed and invasiveness (Lively and Schlichter, 2013; Cougoule et al., 2012). To identify IL-4-induced adhesion, motility and matrix protease gene expression changes, we used AmpliSeq, a reliable and cost-effective method to examine changes in gene expression. However, with primer pairs limited to 20,000, its gene coverage is not as comprehensive as RNA-Seq (Li et al., 2015), as demonstrated by the absence of a widely used M2 marker, *Chil3*. Nevertheless, our IL-4-upregulated gene set matched that of a previous study of IL-4-activated mouse macrophages (Martinez et al., 2013). Overall, gene expression changes in IL-4-treated macrophages were not as marked as those seen with CSF-1-induced differentiation, but striking changes in the regulators of interstitial motility were seen (Fig. 3F, Table 4). Most importantly perhaps were the striking increases in expression of *Mmp12*, *Mmpp13* and *Mmp19*, along with cathepsin K, which are likely to be responsible for the increase in matrix-degrading capacity of IL-4-treated BMMs (Table S12). By increasing their migration and matrix degradation, IL-4 is likely to enhance the ability of TAMs to move through the interstitium *in vivo* and thereby promote invasion of co-migrating tumor cells. TAMs have previously been shown to be a major source of cathepsins B, L and S in the tumor microenvironment (Gocheva et al., 2010). We found that these cathepsins were already abundantly expressed in baseline macrophages with moderate additional IL-4-induced increases demonstrated in cathepsins L and S. Thus, at an RNA level at least, IL-4-treated macrophages express vast quantities of a number of cathepsins along with several MMPs, and, although we do not know the protein levels of these matrix-degrading molecules, IL-4-skewed macrophages are almost certainly very efficient at interstitial migration.

In conclusion, we have comprehensively mapped gene expression changes and measured commensurate increases in adhesion, migration and matrix degradation in macrophages differentiated in the presence of the primary macrophage growth and differentiation factor, CSF-1. Furthermore, we have been able to show definitively that CSF-1-differentiated macrophages are not skewed towards an alternatively activated phenotype but are baseline or ‘M0’ in phenotype. In addition, by extensively characterizing baseline macrophages, we have been able to precisely delineate changes in gene expression and activity of the motility machinery found in IL-4-induced alternatively activated macrophages. Together, these findings are important as macrophages contribute to disease progression in a range of deadly diseases. Furthermore, the identification and selective targeting of core macrophage-specific motility molecules can be used to inhibit the recruitment or activity of disease-enhancing macrophages.

MATERIALS AND METHODS

Macrophage extraction and culture

Bone marrow was flushed from the femurs and tibiae of 8- to 10-week-old male C57BL/6 mice in three independent experiments. All experiments complied with the Australian code for the care and use of animals for scientific purposes and were approved by the University of Western Australia's Animal Ethics Committee. Non-adherent cells were plated in α+ minimum essential medium (MEM; Life Technologies, NY) containing 15% fetal calf serum (FCS; Bovogen, Melbourne, Australia) and a very low dose (0.6 ng/ml) of CSF-1 (kind gift from E. R. Stanley, Albert Einstein College of Medicine, New York, USA) in T75 tissue culture flasks at 37°C and 5% CO_2 to maintain mononuclear phagocytic cell survival as previously described (Tushinski et al., 1982). The following protocol was based on a well-established procedure optimized in the Stanley laboratory that initially enriches for non-adherent mononuclear phagocytic cells in a very low concentration of CSF-1 (0.6 ng/ml) before stimulating synchronous differentiation of the precursor cells into adherent but immature macrophages with an increased dose of CSF-1 (12 ng/ml). Once adherent, BMMs require higher doses of CSF-1 (120 ng/ml), which promotes further maturation (Tushinski et al., 1982). Thus, on day 0, bone marrow-derived cells were plated in 0.6 ng/ml CSF-1 and on day 1, non-adherent cells were collected and resuspended in fresh 0.6 ng/ml CSF-1 medium for a further 24 h before lysis and RNA extraction (Fig. 1A, C1). To produce immature adherent BMMs, on day 2, non-adherent cells were then exposed to 12 ng/ml CSF-1 in α+ MEM and 10% FCS for 4 days (Fig. 1A, C2) (Tushinski et al., 1982). To produce fully mature BMMs, day 1 non-adherent precursor cells were exposed to 12 ng/ml CSF-1 for 48 h then 120 ng/ml CSF-1 for a further 7 days (Fig. 1A, C3) (Tushinski et al., 1982). For IL-4-induced activation, fully mature BMMs were kept in CSF-1 and additionally treated with 20 ng/ml IL-4 (Miltenyi, Macquarie Park, Australia) for 48 h. To ensure viability when splitting adherent cells (2 mm EDTA in PBS), proliferating BMMs were expanded in Petri dishes before plating for at least 2 days on either tissue culture plates (Eppendorf, North Ryde, Australia) for RNA extraction, or fibronectin-coated coverslips (Fisher Biotec, Wembley, Australia) or glass-bottomed dishes (MatTek, Ashland, Australia) for biological assays. At least three biological replicates were carried out for each assay.

Transcriptome and differentially expressed gene analysis

For immature and mature adherent BMMs grown in CSF-1, cells were seeded onto 2×10 cm tissue culture dishes and grown to ∼70% confluence (∼0.5–1×10^6 cells) then lysed and polynucleotides treated with DNase prior to RNA extraction (QIAGEN, Chadstone, Australia). For non-adherent bone marrow-derived precursor cells, a similar number of cells was collected by centrifugation prior to lysis. Eluted RNA from three independent samples for each of the three stages of BMM differentiation and maturation was submitted to the LotteryWest State Biomedical Facility Genomics laboratory at the University of Western Australia for library preparation and sequencing using the Ion Torrent Proton DNA sequencing platform. For each sample, the output fastq files were aligned against the Genome Reference Consortium mouse genome (GRCm38.p6) using the open-source Hisat2 aligner (Kim et al., 2015). The resulting BAM files were uploaded into SeqMonk (version 1.42) with minimum mapping quality set to 60. Aligned sequences passed quality checks outlined in SeqMonk (https://www.bioinformatics.babraham.ac.uk/projects/seqmonk/). PCA analysis and expression scatter plots were generated in SeqMonk using log2 RPM expression. Changes in fold expression were calculated from the log2 RPM data. Lists of differential gene expression were generated using the edgeR platform within SeqMonk using the raw reads as is required in analysis of negative binomial distributions (Schurch et al., 2016). Heatmaps of differentially expressed genes were constructed using the R package pheatmap (Kolde, 2019). For samples treated with and without IL-4, mRNA was again submitted to the LotteryWest State Biomedical Facility Genomics laboratory for conversion to cDNA followed by amplification using the AmpliSeq Mouse Transcriptome V1 PCR primers [Ion AmpliSeq™ Transcriptome Gene Expression Kit mouse (A36553), Life Technologies Australia]. Primers were then partially digested with FuPa and adapters (Ion Xpress™ Barcode Adapters 1-16 Kit, Thermo Fisher Scientific) ligated to amplicons. Libraries were purified, quantitated and six to eight barcoded samples loaded onto chips (Ion PI™, Life Technologies Australia) and sequenced using the Ion S5 System (Thermo Fisher Scientific). Enrichment analysis of the differential gene expression datasets was carried out through GO, using the PANTHER Classification System

(Mi et al., 2016) to identify biological pathways up- or downregulated during differentiation and maturation of macrophages from non-adherent precursors.

Morphology assays

For phase-contrast microscopy, cells were grown on tissue culture dishes then imaged with a Nikon Eclipse TS100 inverted microscope with a Nikon CFl Achromat LWD ADL20xF 0.4 NA objective. For immunofluorescence microscopy, 5.0×10^3 BMMs were seeded onto fibronectin-coated coverslips (Neuvitro, Vancouver, Australia) for 2 days in the appropriate concentration of CSF-1 with or without IL-4, then fixed in 4% paraformaldehyde and permeabilized as described previously (Dwyer et al., 2016). The actin cytoskeleton was stained with Alexa Fluor 568-conjugated phalloidin (Thermo Fisher Scientific) and adhesion structures were stained with an anti-phosphopaxillin pTyr118 antibody (#610051, 1:100, Thermo Fisher Scientific) or a monoclonal anti-paxillin antibody (#610051, 1:200, BD Biosciences) and a polyclonal anti-leupaxin antibody (#STJ111845, 1:100, St John's Laboratory, London, UK) to identify focal complexes and point contacts (Pixley, 2012). Coverslips were mounted in Prolong Diamond with 4′,6-diamidino-2-phenylindole (DAPI; Thermo Fisher Scientific) and imaged on an Olympus IX-81 inverted epifluorescent microscope with an Olympus Plan Apo 60×/1.25 NA oil immersion objective, a Nikon A1 inverted confocal microscope with a Nikon Plan Apo VC 60×/1.49 NA oil immersion objective or a Nikon SIM (Ti2) microscope with a Nikon SR Apo TIRF 100×/1.49 NA oil immersion objective at the Centre for Microscopy, Characterisation and Analysis, University of Western Australia. Images were processed in NIS-Elements (Nikon) and Fiji (Schindelin et al., 2012). To quantify cell footprint area, F-actin stained outlines of at least 50 cells per condition were digitally traced in Fiji. Footprint area (arbitrary units) and elongation (aspect) ratio measurements were calculated and expressed as the mean and s.e.m. for each value. To measure adhesion signal intensity, the mean pY118 paxillin signal was taken from raw data files using Fiji. To quantify adhesion numbers at the leading edge, we adapted the method from Buskermolen et al. (2018) to remove background by thresholding.

Motility assay

For chemotaxis, 1×10^5 BMMs in 100 µl CSF-1-free medium were seeded into 8 µM pore-size transwell chambers (BD Biosciences) and placed into medium with 120 ng/ml CSF-1 in the lower chamber. BMMs were incubated for 6 h before migrated cells on the lower surface of the membrane were fixed and the membranes carefully excised, mounted and imaged with a Nikon Eclipse TS100 inverted microscope at 20× magnification. Cells from ten fields/membrane were counted, averaged and controlled for cell loading by adding 1×10^4 cells to insert-free wells.

Matrix degradation assay

BMMs (2×10^5) were seeded onto Cy3-labelled gelatin-coated 35 mm glass-bottomed dishes in the appropriate dose of CSF-1 plus 20 ng/ml IL-4 for 24 h as described previously (Mouchemore et al., 2013) (Merck, Frenchs Forest, Australia). After fixation and permeabilization, the actin cytoskeleton was stained with Alexa Fluor 488-conjugated phalloidin and nuclei were stained with DAPI. Samples were imaged with five representative fields at 10× magnification by the Olympus IX81 microscope and degraded areas (absence of Cy3 signal) relative to total cell area and total number of cells actively degrading per field were thresholded, quantified and normalized to cell number using ImageJ software.

Transfection of siRNA

Electroporation was performed using the Neon transfection system (Thermo Fisher Scientific) with specific siRNA molecules targeting paxillin (Santa Cruz Biotechnology, sc-36197), leupaxin (Thermo Fisher Scientific, S98816) and a scrambled siRNA (Silencer® Negative Control #2, Thermo Fisher Scientific, AM4613). Electroporation was performed as follows: BMMs were lifted (2 mM EDTA in PBS) and resuspended in buffer R. Two $\times10^5$ cells per transfection were mixed with either 1.0 µM paxillin or 0.8 µM leupaxin or scrambled siRNA and collected in a 100 µl Neon electroporation tip. The microporator was set to a pulse voltage of 1000 V, pulse width of 40 ms and pulse number of 2. Cells were plated as required into pre-warmed growth medium onto fibronectin-coated coverslips or matrix-degradation plates, and allowed to recover for 48 h before fixation and staining for immunofluorescent microscopy.

Statistics

Statistical analyses were carried out in GraphPad Prism. Where necessary, the data were transformed to achieve normality. Unpaired Student's *t*-tests with Welch's correction (Figs 2C,E,G, 3G and 4G) or paired Student's *t*-tests (Fig. 4C) were used in two-way comparisons. One-way (Fig. 4G,H) or two-way (Fig. 4E) analyses of variance (ANOVAs) were used for multiple comparisons. Statistically significant data are denoted by asterisks as follows: *P<0.05, **P<0.01, ***P<0.001 and ****P<0.0001.

Acknowledgements

We acknowledge the facilities, and the scientific and technical assistance of the National Imaging Facility at the Centre for Microscopy, Characterisation and Analysis, the University of Western Australia, with particular gratitude for the help of Alysia Buckley with SIM. We thank Dr Richard Stanley for the kind gift of CSF-1, Michaela Rajarathnan and Nick Peters for their technical assistance, and Dr Wally Langdon and Dr Prue Hart for their critical insights and evaluation of the manuscript.

Competing interests

The authors declare no competing or financial interests.

Author contributions

Conceptualization: M.W.M., J.H.S., E.L.G., D.A.J., F.J.P.; Formal analysis: M.W.M., J.H.S., J.M.P., F.J.P.; Investigation: M.W.M., E.L.G., F.J.P.; Writing - original draft: F.J.P.; Writing - review & editing: M.W.M., J.H.S., D.A.J.; Supervision: F.J.P.; Project administration: F.J.P.; Funding acquisition: F.J.P.

Funding

This work was supported by funding from the Cancer Council Western Australia [APP1078830 and APP1122300 to F.J.P.], the University of Western Australia [Australian Postgraduate Award to M.W.M. and E.L.G.] and the Royal Perth Hospital Medical Research Foundation.

Data availability

Raw RNA-Seq data have been deposited in GEO under accession number GSE145437.

Supplementary information

Supplementary information available online at http://jcs.biologists.org/lookup/doi/10.1242/jcs.232405.supplemental

References

Abram, C. L. and Lowell, C. A. (2008). The diverse functions of Src family kinases in macrophages. *Front. Biosci.* **13**, 4426-4450. doi:10.2741/3015

Allen, W. E., Jones, G. E., Pollard, J. W. and Ridley, A. J. (1997). Rho, Rac and Cdc42 regulate actin organization and cell adhesion in macrophages. *J. Cell Sci.* **110**, 707-720.

Buskermolen, A. B. C., Kurniawan, N. A. and Bouten, C. V. C. (2018). An automated quantitative analysis of cell, nucleus and focal adhesion morphology. *PLoS ONE* **13**, e0195201. doi:10.1371/journal.pone.0195201

Bustelo, X. R., Sauzeau, V. and Berenjeno, I. M. (2007). GTP-binding proteins of the Rho/Rac family: regulation, effectors and functions in vivo. *BioEssays* **29**, 356-370. doi:10.1002/bies.20558

Cheng, F. and Eriksson, J. E. (2017). Intermediate filaments and the regulation of cell motility during regeneration and wound healing. *Cold Spring Harb. Perspect. Biol.* **9**, a022046. doi:10.1101/cshperspect.a022046

Cougoule, C., Van Goethem, E., Le Cabec, V., Lafouresse, F., Dupré, L., Mehraj, V., Mège, J.-L., Lastrucci, C. and Maridonneau-Parini, I. (2012). Blood leukocytes and macrophages of various phenotypes have distinct abilities to form podosomes and to migrate in 3D environments. *Eur. J. Cell Biol.* **91**, 938-949. doi:10.1016/j.ejcb.2012.07.002

Deakin, N. O., Pignatelli, J. and Turner, C. E. (2012). Diverse roles for the paxillin family of proteins in cancer. *Genes Cancer* **3**, 362-370. doi:10.1177/1947601912458582

DeNardo, D. G., Barreto, J. B., Andreu, P., Vasquez, L., Tawfik, D., Kolhatkar, N. and Coussens, L. M. (2009). CD4+ T cells regulate pulmonary metastasis of mammary carcinomas by enhancing protumor properties of macrophages. *Cancer Cell.* **16**, 91-102. doi:10.1016/j.ccr.2009.06.018

Devreotes, P. and Horwitz, A. R. (2015). Signaling networks that regulate cell migration. *Cold Spring Harb. Perspect. Biol.* **7**, a005959. doi:10.1101/cshperspect.a005959

Dwyer, A. R., Mouchemore, K. A., Steer, J. H., Sunderland, A. J., Sampaio, N. G., Greenland, E. L., Joyce, D. A. and Pixley, F. J. (2016). Src family kinase expression and subcellular localization in macrophages: implications for their role in CSF-1-induced macrophage migration. *J. Leukoc. Biol.* **100**, 163-175. doi:10.1189/jlb.2A0815-344RR

Frantz, C., Stewart, K. M. and Weaver, V. M. (2010). The extracellular matrix at a glance. *J. Cell Sci.* **123**, 4195-4200. doi:10.1242/jcs.023820

Friedl, P. and Wolf, K. (2010). Plasticity of cell migration: a multiscale tuning model. *J. Cell Biol.* **188**, 11-19. doi:10.1083/jcb.200909003

Gautier, E. L., Shay, T., Miller, J., Greter, M., Jakubzick, C., Ivanov, S., Helft, J., Chow, A., Elpek, K. G., Gordonov, S. et al. (2012). Gene-expression profiles and transcriptional regulatory pathways that underlie the identity and diversity of mouse tissue macrophages. *Nat. Immunol.* **13**, 1118-1128. doi:10.1038/ni.2419

Gocheva, V., Wang, H.-W., Gadea, B. B., Shree, T., Hunter, K. E., Garfall, A. L., Berman, T. and Joyce, J. A. (2010). IL-4 induces cathepsin protease activity in tumor-associated macrophages to promote cancer growth and invasion. *Genes Dev.* **24**, 241-255. doi:10.1101/gad.1874010

Guiet, R., Van Goethem, E., Cougoule, C., Balor, S., Valette, A., Al Saati, T., Lowell, C. A., Le Cabec, V. and Maridonneau-Parini, I. (2011). The process of macrophage migration promotes matrix metalloproteinase-independent invasion by tumor cells. *J. Immunol.* **187**, 3806-3814. doi:10.4049/jimmunol.1101245

Han, X., Wang, R., Zhou, Y., Fei, L., Sun, H., Lai, S., Saadatpour, A., Zhou, Z., Chen, H., Ye, F. et al. (2018). Mapping the mouse cell atlas by microwell-Seq. *Cell* **172**, 1091-1107. doi:10.1016/j.cell.2018.02.001

Horne-Badovinac, S. (2017). Fat-like cadherins in cell migration-leading from both the front and the back. *Curr. Opin. Cell Biol.* **48**, 26-32. doi:10.1016/j.ceb.2017.04.003

Horton, E. R., Byron, A., Askari, J. A., Ng, D. H. J., Millon-Frémillon, A., Robertson, J., Koper, E. J., Paul, N. R., Warwood, S., Knight, D. et al. (2015). Definition of a consensus integrin adhesome and its dynamics during adhesion complex assembly and disassembly. *Nat. Cell Biol.* **17**, 1577-1587. doi:10.1038/ncb3257

Horton, E. R., Humphries, J. D., James, J., Jones, M. C., Askari, J. A. and Humphries, M. J. (2016). The integrin adhesome network at a glance. *J. Cell Sci.* **129**, 4159-4163. doi:10.1242/jcs.192054

Hyder, C. L., Lazaro, G., Pylvänäinen, J. W., Roberts, M. W. G., Qvarnström, S. M. and Eriksson, J. E. (2014). Nestin regulates prostate cancer cell invasion by influencing the localisation and functions of FAK and integrins. *J. Cell Sci.* **127**, 2161-2173. doi:10.1242/jcs.125062

Hynes, R. O. and Naba, A. (2012). Overview of the matrisome - an inventory of extracellular matrix constituents and functions. *Cold Spring Harb. Perspect. Biol.* **4**, a004903. doi:10.1101/cshperspect.a004903

Jablonski, K. A., Amici, S. A., Webb, L. M., Ruiz-Rosado, J. D., Popovich, P. G., Partida-Sanchez, S. and Guerau-de-Arellano, M. (2015). Novel markers to delineate murine M1 and M2 macrophages. *PLoS ONE* **10**, e0145342. doi:10.1371/journal.pone.0145342

Kim, D., Langmead, B. and Salzberg, S. L. (2015). HISAT: a fast spliced aligner with low memory requirements. *Nat. Methods.* **12**, 357-360. doi:10.1038/nmeth.3317

Klapproth, S., Bromberger, T., Türk, C., Krüger, M. and Moser, M. (2019). A kindlin-3-leupaxin-paxillin signaling pathway regulates podosome stability. *J. Cell Biol.* **218**, 3436-3454. doi:10.1083/jcb.201903109

Kolde, R. (2019). Pheatmap: Pretty heatmaps. R package version 1.0.1 https://CRAN.R-project.org/package=pheatmap.

Krishnasamy, S., Weng, Y.-C., Thammisetty, S. S., Phaneuf, D., Lalancette-Hebert, M. and Kriz, J. (2017). Molecular imaging of nestin in neuroinflammatory conditions reveals marked signal induction in activated microglia. *J. Neuroinflammation* **14**, 45. doi:10.1186/s12974-017-0816-7

Krol, A., Henle, S. J. and Goodrich, L. V. (2016). Fat3 and Ena/VASP proteins influence the emergence of asymmetric cell morphology in the developing retina. *Development* **143**, 2172-2182. doi:10.1242/dev.133678

Lauffenburger, D. A. and Horwitz, A. F. (1996). Cell migration: a physically integrated molecular process. *Cell* **84**, 359-369. doi:10.1016/S0092-8674(00)81280-5

Li, W., Turner, A., Aggarwal, P., Matter, A., Storvick, E., Arnett, D. K. and Broeckel, U. (2015). Comprehensive evaluation of AmpliSeq transcriptome, a novel targeted whole transcriptome RNA sequencing methodology for global gene expression analysis. *BMC Genomics* **16**, 1069. doi:10.1186/s12864-015-2270-1

Lin, E. Y., Nguyen, A. V., Russell, R. G. and Pollard, J. W. (2001). Colony-stimulating factor 1 promotes progression of mammary tumors to malignancy. *J. Exp. Med.* **193**, 727-740. doi:10.1084/jem.193.6.727

Linder, S. and Wiesner, C. (2015). Tools of the trade: podosomes as multipurpose organelles of monocytic cells. *Cell Mol. Life Sci.* **72**, 121-135. doi:10.1007/s00018-014-1731-z

Lipsky, B. P., Beals, C. R. and Staunton, D. E. (1998). Leupaxin is a novel LIM domain protein that forms a complex with Pyk2. *J. Biol. Chem.* **273**, 11709-11713. doi:10.1074/jbc.273.19.11709

Lively, S. and Schlichter, L. C. (2013). The microglial activation state regulates migration and roles of matrix-dissolving enzymes for invasion. *J. Neuroinflammation.* **10**, 75. doi:10.1186/1742-2094-10-75

Lund, S. A., Wilson, C. L., Raines, E. W., Tang, J., Giachelli, C. M. and Scatena, M. (2013). Osteopontin mediates macrophage chemotaxis via α4 and α9 integrins and survival via the α4 integrin. *J. Cellul. Biochem.* **114**, 1194-1202. doi:10.1002/jcb.24462

Martinez, F. O. and Gordon, S. (2014). The M1 and M2 paradigm of macrophage activation: time for reassessment. *F1000Prime Rep.* **6**, 13-25. doi:10.12703/P6-13

Martinez, F. O., Helming, L., Milde, R., Varin, A., Melgert, B. N., Draijer, C., Thomas, B., Fabbri, M., Crawshaw, A., Ho, L. P. et al. (2013). Genetics programs expressed in resting and alternatively activated mouse and human macrophages: similarities and differences. *Blood* **121**, e57-e69. doi:10.1182/blood-2012-06-436212

McWhorter, F. Y., Wang, T., Nguyen, P., Chung, T. and Liu, W. F. (2013). Modulation of macrophage phenotype by cell shape. *Proc. Natl. Acad. Sci. USA* **110**, 17253-17258. doi:10.1073/pnas.1308887110

Mi, H., Huang, X., Muruganujan, A., Tang, H., Mills, C. D., Kang, D. and Thomas, P. D. (2016). PANTHER version 11: expanded annotation data from Gene Ontology and Reactome pathways, and data analysis tool enhancements. *Nucleic Acids Res.* **45**, D183-D189. doi:10.1093/nar/gkw1138

Mosser, D. M. and Edwards, J. P. (2008). Exploring the full spectrum of macrophage activation. *Nat. Rev. Immunol.* **8**, 958-969. doi:10.1038/nri2448

Mouchemore, K. A., Sampaio, N. G., Murrey, M. W., Stanley, E. R., Lannutti, B. J. and Pixley, F. J. (2013). Specific inhibition of PI3K p110δ inhibits CSF-1-induced macrophage spreading and invasive capacity. *FEBS J.* **280**, 5228-5236. doi:10.1111/febs.12316

Murray, P. J., Allen, J. E., Biswas, S. K., Fisher, E. A., Gilroy, D. W., Goerdt, S., Gordon, S., Hamilton, J. A., Ivashkiv, L. B., Lawrence, T. et al. (2014). Macrophage activation and polarization: nomenclature and experimental guidelines. *Immunity* **41**, 14-20. doi:10.1016/j.immuni.2014.06.008

Newby, A. C. (2016). Metalloproteinase production from macrophages - a perfect storm leading to atherosclerotic plaque rupture and myocardial infarction. *Exp. Physiol.* **101**, 1327-1337. doi:10.1113/EP085567

Okabe, Y. and Medzhitov, R. (2015). Tissue biology perspective on macrophages. *Nat. Immunol.* **17**, 9-17. doi:10.1038/ni.3320

Owen, K. A., Pixley, F. J., Thomas, K. S., Vincente-Manzanares, M., Ray, B. J., Horwitz, A. J., Parsons, J. T., Beggs, H. E., Stanley, E. R. and Bouton, A. H. (2007). Regulation of lamellipodial persistence, adhesion turnover, and motility in macrophages by focal adhesion kinase. *J. Cell Biol.* **179**, 1275-1287. doi:10.1083/jcb.200708093

Perdiguero, E. G. and Geissmann, F. (2015). The development and maintenance of resident macrophages. *Nat. Immunol.* **17**, 2-8. doi:10.1038/ni.3341

Pixley, F. J. (2012). Macrophage migration and its regulation by CSF-1. *Int. J. Cell Biol.* **2012**, 501962. doi:10.1155/2012/501962

Pixley, F. J. and Stanley, E. R. (2004). CSF-1 regulation of the wandering macrophage: complexity in action. *Trend Cell Biol.* **14**, 628-638. doi:10.1016/j.tcb.2004.09.016

Pixley, F. J., Lee, P. S. W., Condeelis, J. S. and Stanley, E. R. (2001). Protein tyrosine phosphatase ϕ regulates paxillin tyrosine phosphorylation and mediates colony-stimulating factor 1-induced morphological changes in macrophages. *Mol. Cell. Biol.* **21**, 1795-1809. doi:10.1128/MCB.21.5.1795-1809.2001

Ridley, A. J. (2011). Life at the leading edge. *Cell* **145**, 1012-1022. doi:10.1016/j.cell.2011.06.010

Sampaio, N. G., Yu, W., Cox, D., Wyckoff, J., Condeelis, J., Stanley, E. R. and Pixley, F. J. (2011). Phosphorylation of CSF-1R Y721 mediates its association with PI3K to regulate macrophage motility and enhancement of tumor cell invasion. *J. Cell Sci.* **124**, 2021-2031. doi:10.1242/jcs.075309

Schindelin, J., Arganda-Carreras, I., Frise, E., Kaynig, V., Longair, M., Pietzsch, T., Preibisch, S., Rueden, C., Saalfeld, S., Schmid, B. et al. (2012). Fiji: an open-source platform for biological-image analysis. *Nat. Methods* **9**, 676-682. doi:10.1038/nmeth.2019

Schridde, A., Bain, C. C., Mayer, J. U., Montgomery, J., Pollet, E., Denecke, B., Milling, S. W. F., Jenkins, S. J., Dalod, M., Henri, S. et al. (2017). Tissue-specific differentiation of colonic macrophages requires TGFβ receptor-mediated signaling. *Mucosal Immunol.* **10**, 1387-1399. doi:10.1038/mi.2016.142

Schurch, N. J., Schofield, P., Gierliński, M., Cole, C., Sherstnev, A., Singh, V., Wrobel, N., Gharbi, K., Simpson, G. G., Owen-Hughs, T. et al. (2016). How many biological replicates are needed in an RNA-seq experiment and which differential expression tool should you use? *RNA* **22**, 839-851. doi:10.1261/rna.053959.115

Sullivan, A. R. and Pixley, F. J. (2014). CSF-1R signaling in health and disease: a focus on the mammary gland. *J. Mammary Gland Biol. Neoplasia.* **19**, 149-159. doi:10.1007/s10911-014-9320-1

Suzuki, H., Forrest, A. R., van Nimwegen, E., Daub, C. O., Balwierz, P. J., Irvine, K. M., Lassmann, T., Ravasi, T., Hasegawa, Y., de Hoon, M. J. L. et al. (2009). The transcriptional network that controls growth arrest and differentiation in a human myeloid leukemia cell line. *Nat. Genet.* **41**, 553-562. doi:10.1038/ng.375

Tushinski, R. J., Oliver, I. T., Guilbert, L. J., Tynan, P. W., Warner, J. R. and Stanley, E. R. (1982). Survival of mononuclear phagocytes depends on a lineage-

specific growth factor that the differentiated cells selectively destroy. *Cell* **28**, 71-81. doi:10.1016/0092-8674(82)90376-2

Van den Bossche, J., Malissen, B., Mantovani, A., De Baetselier, P. and Van Ginderachter, J. A. (2012). Regulation and function of the E-cadherin/catenin complex in cells of the monocyte-macrophage lineage and DCs. *Blood* **119**, 1623-1633. doi:10.1182/blood-2011-10-384289

Van Goethem, E., Poincloux, R., Gauffre, F., Maridonneau-Parini, I. and Le Cabec, V. (2010). Matrix architecture dictates three-dimensional migration modes of human macrophages: differential involvement of proteases and podosome-like structures. *J. Immunol.* **184**, 1049-1061. doi:10.4049/jimmunol.0902223

Vérollet, C., Charrière, G. M., Labrousse, A., Cougoule, C., Le Cabec, V. and Maridonneau-Parini, I. (2011). Extracellular proteolysis in macrophage migration: Losing grip for a breakthrough. *Eur. J. Immunol.* **41**, 2805-2813. doi:10.1002/eji.201141538

Vogel, D. Y. S., Heijnen, P. D. A. M., Breur, M., de Vries, H. E., Tool, A. T., Amor, S. and Dijkstra, C. D. (2014). Macrophages migrate in an activation-dependent manner to chemokines involved in neuroinflammation. *J. Neuroinflammation* **11**, 23-33. doi:10.1186/1742-2094-11-23

Webb, S. E., Pollard, J. W. and Jones, G. E. (1996). Direct observation and quantification of macrophage chemoattraction to the growth factor CSF-1. *J. Cell Sci.* **109**, 793-803.

Weerasinghe, D., McHugh, K. P., Ross, F. P., Brown, E. J., Gisler, R. H. and Imhof, B. A. (1998). A role for the alphavbeta3 integrin in the transmigration of monocytes. *J. Cell Biol.* **142**, 595-607. doi:10.1083/jcb.142.2.595

Wei, S., Nandi, S., Chitu, V., Yeung, Y.-G., Yu, W., Huang, M., Williams, L. T., Lin, H. and Stanley, E. R. (2010). Functional overlap but differential expression of CSF-1 and IL-34 in their CSF-1 receptor-mediated regulation of myeloid cells. *J. Leukoc. Biol.* **88**, 495-505. doi:10.1189/jlb.1209822

Winograd-Katz, S. E., Fässler, R., Geiger, B. and Legate, K. R. (2014). The integrin adhesome: from genes and proteins to human disease. *Nat. Rev. Mol. Cell Biol.* **15**, 273-288. doi:10.1038/nrm3769

Wyckoff, J., Wang, W., Lin, E. Y., Wang, Y., Pixley, F. J., Stanley, E. R., Graf, T., Pollard, J. W., Segall, J. and Condeelis, J. (2004). A paracrine loop between tumor cells and macrophages is required for tumor cell migration in mammary tumors. *Cancer Res.* **64**, 7022-7029. doi:10.1158/0008-5472.CAN-04-1449

Wyckoff, J. B., Wang, Y., Goswami, S., Wang, Y., Sidani, M., Segall, J. E. and Condeelis, J. S. (2007). Direct visualization of macrophage-assisted tumor cell intravasation in mammary tumors. *Cancer Res.* **67**, 2649-2656. doi:10.1158/0008-5472.CAN-06-1823

Wynn, T. A., Chawla, A. and Pollard, J. W. (2013). Macrophage biology in development, homeostasis and disease. *Nature* **496**, 445-455. doi:10.1038/nature12034

Xue, J., Schmidt, S. V., Sander, J., Draffehn, A., Krebs, W., Quester, I., De Nardo, D., Gohel, T. D., Emde, M., Schmidleithner, L. et al. (2014). Transcriptome-based network analysis reveals a spectrum model of human macrophage activation. *Immunity* **40**, 274-288. doi:10.1016/j.immuni.2014.01.006

Yang, M., McKay, D., Pollard, J. W. and Lewis, C. E. (2018). Diverse functions of macrophages in different tumor microenvironments. *Cancer Res.* **78**, 5492-5503. doi:10.1158/0008-5472.CAN-18-1367

Yu, W., Chen, J., Xiong, Y., Pixley, F. J., Dai, X.-M., Yeung, Y.-G. and Stanley, E. R. (2008). CSF-1 receptor structure/function in MacCsf1r−/− macrophages: regulation of proliferation, differentiation, and morphology. *J. Leukoc. Biol.* **84**, 852-863. doi:10.1189/jlb.0308171

Yuan, H., He, J., Zhang, G., Zhang, D., Kong, X. and Chen, F. (2017). Osteoclast stimulatory transmembrane protein induces a phenotypic switch in macrophage polarization suppressing an M1 pro-inflammatory state. *Acta Biochim. Biophys. Sin.* **49**, 935-944. doi:10.1093/abbs/gmx092

Zaidel-Bar, R., Milo, R., Kam, Z. and Geiger, B. (2007). A paxillin tyrosine phosphorylation switch regulates the assembly and form of cell-matrix adhesions. *J. Cell Sci.* **120**, 137-148. doi:10.1242/jcs.03314

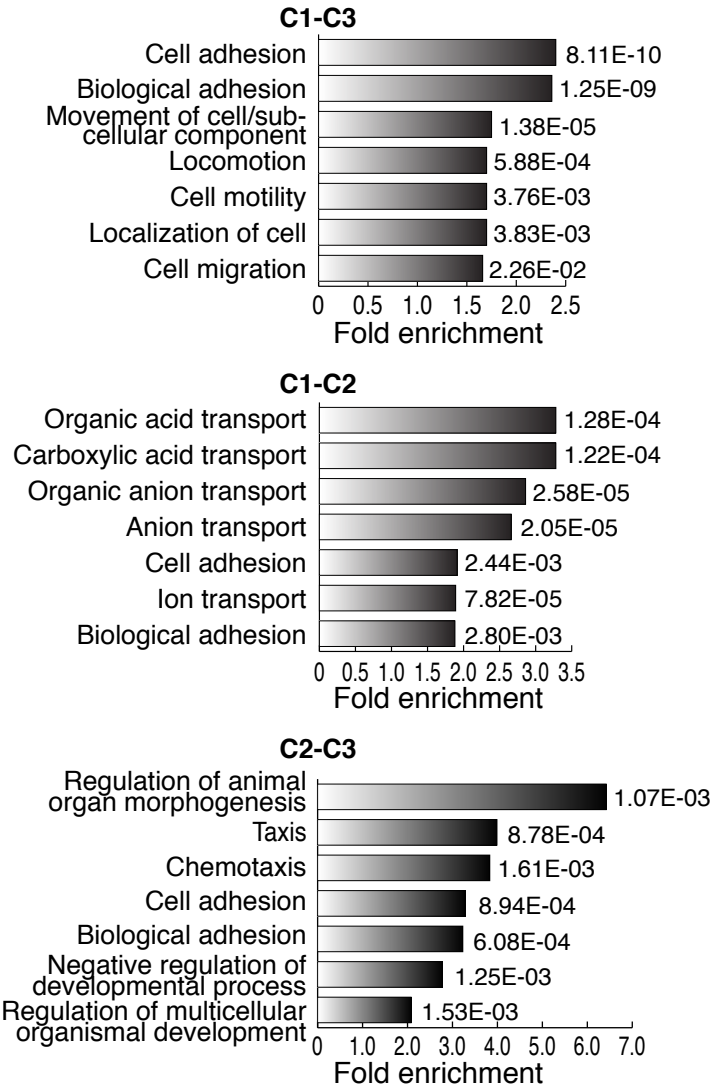

Figure S1. GO functional analysis shows enrichment of adhesion and motility pathways. The top upregulated biological pathways for CSF-1-induced macrophage differentiation for overall differentiation (C1 to C3), development of adhesion from non-adherent precursors (C1 to C2) and subsequent maturation of adherent macrophages (C2 to C3). Fold-enrichment is on the X-axis and the p value is beside each pathway.

List of supplementary tables:

Table S1 - Numbers of differentially expressed genes during CSF-1-induced differentiation

Table S2 - Top 50 downregulated and upregulated genes

Table S3 - Genes significantly up- or down-regulated, C1-C3 differentiation

Table S4 - Genes significantly up- or down-regulated, C1-C2 differentiation

Table S5 - Genes significantly up- or down-regulated, C2-C3 differentiation

Table S6 - Han *in vivo* macrophage cluster matches

Table S7 - Integrated Adhesome

Table S8 - Cadherins and catenins

Table S9 - Rho family GAPs and GEFs

Table S10 - Rho family actin effectors

Table S11 - Intermediate filaments

Table S12 – Differentially expressed genes during IL-4-induced activation

Table S13 - Core adhesion gene expression changes during IL-4-induced activation

Table S1. Numbers of differentially expressed genes (p<0.01)

Differentiation Stage	Upregulated	Downregulated	Total
C1 to C3	2407	3355	5752
C1 to C2	2415	3582	5997
C2 to C3	487	554	1041

Table S2. Top 50 down- and up-regulated genes

C3/C1 down		C3/C1 up		C2/C1 down		C2/C1 up		C3/C2 down		C3/C2 up	
Gene	Ratio	Gene	Ratio	Gene	Ratio	Gene	Ratio	Gene	Ratio	Gene	Ratio
S100a9	0.00001	Nes	2661.95	Mmp9	0.00016	Speg	971.70	Scd1	0.0008	Trem1	274.90
Ngp	0.00002	Fat3	2180.81	Retnlg	0.00029	Fcna	325.08	S100a9	0.0011	Id1	239.71
Ltf	0.00006	Speg	1740.90	Hbb-bs	0.00073	Pmp22	296.82	Scd2	0.0023	Cd207	147.39
Mpo	0.00009	Ch25h	1169.49	Cd79a	0.00087	Adra1a	255.18	Ngp	0.0024	Ch25h	110.48
Chil3	0.00010	Emp2	1066.19	Fn1	0.00088	Gas6	241.43	F13a1	0.0024	Zfp618	108.72
Lcn2	0.00010	Fcna	953.98	Cxcr2	0.00104	Folr2	206.41	H2-Aa	0.0025	Ltbp2	97.86
Camp	0.00012	Folr2	879.49	Cd19	0.00110	Lama3	182.26	Chil3	0.0032	Pcsk1	70.34
Ly6c2	0.00015	Htr2b	573.53	Nt5e	0.00128	Cacna1a	166.17	H2-Eb1	0.0044	Id3	52.90
Sell	0.00022	P4ha2	467.68	Ikzf3	0.00137	Lrrc14b	156.20	Camp	0.0055	Dmwd	52.90
Cd177	0.00024	Pmp22	385.09	Mmp25	0.00143	Emp2	155.70	Ciita	0.0056	Sox7	52.82
S100a8	0.00026	Cdkn2a	379.98	Rag1	0.00156	Gpr176	137.68	Ccr2	0.0065	Gm26902	51.38
H2-Aa	0.00027	Lama3	359.01	Mctp2	0.00156	Samd4	128.25	Fads2	0.0071	Adcy2	50.25
Itgb2l	0.00029	Edil3	310.18	Il1f9	0.00162	Nes	125.01	Mpo	0.0075	Epha2	48.80
Retnlg	0.00029	Kitl	307.39	Pax5	0.00166	4930430E1	123.53	Ltf	0.0078	Ccnd1	48.06
Cxcr2	0.00030	Cacna1a	307.25	Fcmr	0.00182	Asb4	120.13	Gpr141	0.0086	Pmepa1	41.44
Prtn3	0.00034	Hmga2	298.91	Cecr2	0.00183	Htr2b	118.02	Ly6c2	0.0090	Synpo	39.68
Plbd1	0.00037	Pla2g5	289.33	Zfp831	0.00189	Gdf15	114.79	Clec2i	0.0093	Nptx1	37.77
F13a1	0.00040	Shc2	284.66	Asprv1	0.00199	Fat3	113.39	Treml2	0.0094	AA467197	37.50
Rab44	0.00040	Nrcam	279.15	Ablim1	0.00217	Cnrip1	112.43	Ms4a4a	0.0102	Tmeff1	34.22
Plac8	0.00042	Cpe	276.23	Hbb-bt	0.00220	Gpr162	110.25	H2-Ab1	0.0104	Sncaip	31.18
Ctsg	0.00044	Gas6	251.11	Nlrp12	0.00221	Kitl	106.80	Adam19	0.0105	Pxdc1	30.07
Hp	0.00045	Zfp618	247.14	Hba-a1	0.00224	Pdgfc	99.61	Plbd1	0.0110	Spsb1	28.15
H2-Eb1	0.00047	Meis3	214.19	Amer2	0.00230	Gprc5c	97.63	Thbs1	0.0115	Cdkn2a	25.79
Fn1	0.00053	Cdkn2b	203.48	Apol7c	0.00242	Cmbl	88.30	F7	0.0137	Galnt3	25.77
Ccdc88c	0.00053	Vsig4	197.64	Mgam	0.00244	Mcoln3	84.81	Ptger3	0.0149	Stard13	25.26
Myb	0.00058	Spats2	156.66	Ms4a1	0.00269	P4ha2	81.01	Phgdh	0.0158	Cxcl14	25.18
Elane	0.00067	Pcdhac2	143.76	Tinagl1	0.00278	Naprt	80.56	Lrrc14b	0.0169	Hectd2os	24.83
Ciita	0.00072	Nptx1	141.54	Atp1b1	0.00280	Cpeb1	78.47	Lcn2	0.0177	Atf7ip2	24.30
Hbb-bs	0.00075	Epas1	139.91	Blk	0.00289	Mt2	78.14	Cd177	0.0182	Col14a1	24.26
Chil1	0.00078	G530011C	136.41	Pou2af1	0.00290	Eya4	77.50	Mmp8	0.0186	Vsig4	22.03
Prg2	0.00080	Ccl12	135.04	Trem1	0.00304	Unc5b	76.69	Axl	0.0191	Nes	21.29
Rflnb	0.00082	Cpeb1	127.66	Fpr1	0.00309	Gdpd1	75.27	Elane	0.0192	Plxna4	21.21
Thbs1	0.00084	Plekhh2	121.39	Bach2	0.00313	Cd300ld4	74.17	Plac8	0.0200	Cdkn2b	21.01
Mmp9	0.00086	Rgs11	114.76	Ebf1	0.00317	C77080	73.84	Klk1b11	0.0202	Hcar2	19.32
Treml2	0.00088	Slc9b2	114.53	Cpm	0.00321	Stab2	73.70	Rab44	0.0216	Fat3	19.23
Cd79a	0.00088	Cd59a	113.91	Fscn1	0.00332	Spats2	70.44	Ctsg	0.0228	Gm38248	18.52
Satb1	0.00089	Rab34	112.86	Ccr7	0.00333	Meis3	70.39	Prtn3	0.0238	Nanos1	18.08
Pglyrp1	0.00092	Sh3bgrl2	109.97	Itih5	0.00338	Lamb2	65.07	Kmo	0.0241	Dusp4	17.99
F5	0.00097	Gsta3	108.72	Cacna1e	0.00339	Ednrb	63.78	Smpd3	0.0247	Ndst3	17.69
Flt3	0.00111	Bik	104.61	Ly6g	0.00362	Neil2	63.05	Cd74	0.0251	Flt1	17.64
Cd19	0.00112	Creg2	104.11	Pik3c2b	0.00371	Cdk15	62.91	Ms4a4c	0.0269	Asb2	17.57
Itga2b	0.00112	Adra1a	103.92	Gm43181	0.00374	Shc2	62.42	S100a8	0.0277	Gm807	17.57
H2-Ab1	0.00115	Hectd2os	102.62	Prss34	0.00376	Peli3	61.86	Hp	0.0278	Phlda1	16.83
Siglech	0.00116	Rhod	102.28	Ankrd22	0.00376	2210011C2	58.48	Itga2b	0.0283	Ccl12	16.01
Ccr2	0.00120	Zcchc14	101.30	Tnfrsf13c	0.00401	Serpinb6a	58.42	Jaml	0.0288	Cpe	15.94
Cd79b	0.00121	Ctsf	100.34	Ppp1r16b	0.00423	Gm15513	58.13	Sell	0.0298	Dnm1	14.63
Chst15	0.00122	Lipn	99.64	Aff3	0.00425	Cd300ld2	57.19	Mefv	0.0311	Klra2	14.54
Nedd4	0.00123	Cmbl	97.17	Cd55	0.00430	Zcchc14	55.00	Ppbp	0.0316	Pilra	14.53
Crispld2	0.00125	Efr3b	96.73	Mast4	0.00442	Mmp27	54.54	Itgb2l	0.0324	Ccl2	14.48
Pax5	0.00125	Eya4	96.47	Myb	0.00447	Hmga2	53.86	Tlr9	0.0325	Prss46	14.47

Table S3 - Genes significantly up- or down-regulated, C1-C3 differentiation

Click here to Download Table S3

Table S4 - Genes significantly up- or down-regulated, C1-C2 differentiation

Click here to Download Table S4

Table S5 - Genes significantly up- or down-regulated, C2-C3 differentiation

Click here to Download Table S5

Table S6. Genes up-regulated in C1 to C3 that match Mouse Cell Atlas macrophage markers

Markers common to all 4 Han Mϕ clusters AND up-regulated in C1 to C3	**C3/C1**	**C1 RPM** Mean log2	**C2 RPM** Mean log 2	**C3 RPM** Mean log2	**C1 Reads** Mean raw	**C2 Reads** Mean raw	**C3 Reads** Mean raw
C1qa	47.62	5.16	8.97	10.74	963.3	6764.3	28197.0
C1qc	20.88	6.01	9.88	10.40	1692.3	12598.7	22726.3
Mrc1	14.78	5.76	10.37	9.65	1202.3	17183.3	13842.7
Fcgrt	11.45	3.65	7.19	7.17	294.7	2397.7	2629.7
Adgre1	10.03	7.36	10.12	10.69	3582.7	16183.0	27901.3
C1qb	9.32	7.71	10.70	10.93	4837.7	23731.3	33131.3
Ctsd	8.51	10.62	12.88	13.71	29677.7	142626.7	273244.7
Ctsb	7.38	10.27	13.34	13.16	25231.7	170676.3	180398.3
Lgmn	5.48	7.49	10.68	9.95	4088.3	22752.3	16381.0
Selenop	4.87	7.78	11.32	10.07	4367.7	56047.3	18915.7
Hexa	4.83	7.58	9.95	9.85	3981.7	14506.7	16934.0
Ctss	4.83	8.47	10.39	10.74	7636.3	20552.0	28700.0
Bst2	4.38	5.72	7.36	7.85	1382.7	2164.3	3463.3
Ctsa	4.05	7.72	9.56	9.74	4386.0	10435.7	14239.3
Sdcbp	3.99	7.62	9.86	9.61	4041.3	12663.0	12567.3
Cd68	3.82	6.79	9.00	8.73	2555.0	7355.3	7545.7
Blvrb	3.31	6.81	8.15	8.54	2590.3	3766.7	5843.0
Grn	3.24	8.65	10.71	10.35	8655.3	23855.7	22231.0
Npc2	3.18	7.35	9.26	9.01	3489.3	8499.7	8817.3
Creg1	3.15	7.87	9.05	9.53	4758.7	7737.0	13033.3
Atp6v0b	3.14	6.36	7.77	8.00	1832.0	2898.3	4230.7
Cstb	3.11	5.30	7.26	6.94	944.0	2061.7	1826.7
Lgals3	2.93	9.58	11.40	11.13	15302.3	41882.3	40639.0
Maf	2.85	6.14	7.77	7.66	1712.3	2939.7	3290.7
Ctsz	2.76	8.73	10.35	10.19	9121.7	18389.7	19935.0
Atp6ap1	2.66	6.95	8.35	8.36	2578.0	4343.0	5236.7
Fcgr3	2.65	7.98	9.45	9.38	5001.7	10507.7	11693.3
Clta	2.62	7.51	8.81	8.89	3830.0	5797.0	7636.7
Akr1a1	2.51	7.99	10.20	9.31	5295.3	16591.7	10114.3
Lamp1	2.43	9.11	10.92	10.39	10687.3	31359.0	22440.7
Snx2	2.27	7.15	7.87	8.33	3142.0	3088.7	4800.3
Lyz2	2.25	13.04	13.88	14.21	122126.0	227381.7	478054.0
Itm2b	1.90	9.13	10.31	10.06	10749.7	22698.0	17474.0
Fth1	1.90	9.57	10.90	10.50	16503.0	30483.0	23565.3
Ostf1	1.88	7.65	8.14	8.56	4057.3	3656.3	5833.3
Ptpn18	1.82	5.56	6.20	6.43	1028.0	952.7	1242.3
Calm1	1.79	8.99	9.45	9.83	10364.7	9231.0	14989.3
Cyba	1.73	7.45	8.30	8.25	3708.0	4176.0	4869.7
Snx5	1.73	7.62	9.29	8.41	4033.7	8650.0	5089.3
Cfp	1.67	7.72	8.36	8.46	4405.3	4327.3	5927.3
Cd53	1.56	7.51	7.81	8.15	3694.7	3216.3	4450.7
Csf1r	1.52	9.70	10.87	10.30	16113.3	30946.0	21370.3
Ftl1	1.16	11.72	12.00	11.93	51400.7	68989.3	76498.0
Tmsb4x	1.07	12.33	11.29	12.44	69927.3	37345.0	96815.3

Table S7 - Integrated Adhesome

Click here to Download Table S7

Table S8 - Cadherins and catenins

Protein	Gene	C3 / C1	p value	C2 / C1	p value	C3 / C2	p value	Mean Log2 RPM		
								C1	C2	C3
E-Cadherin	Cdh1	0.02	0.001	0.00	0.001	3.39	ns	3.65	-4.07	-2.31
Cadherin 23	Cdh23	0.05	0.001	0.07	0.001	0.78	ns	0.50	-3.38	-3.73
Dachsous1	Dach1	0.12	0.001	0.01	0.001	10.85	0.01	3.37	-3.09	0.35
Fat3	Fat3	2183.04	0.001	113.40	0.001	19.25	0.001	-3.67	3.16	7.43
Celsr1	Celsr1	0.01	0.001	0.02	0.001	0.51	ns	2.76	-3.07	-4.05
Celsr2	Celsr2	1.22	ns	0.19	0.001	6.41	0.05	-0.07	-2.47	0.21
Flamingo/Celsr3	Celsr3	0.19	0.001	0.33	0.001	0.58	ns	3.51	1.89	1.10
Protocadherin 7	Pcdh7	30.45	0.001	4.32	0.01	7.05	0.001	2.06	4.17	6.99
Protocadherin α1	Pcdha1	47.55	0.001	12.59	0.001	3.78	0.01	-4.10	-0.45	1.47
α-catenin/αE-catenin	Ctnna1	1.67	0.01	1.81	0.001	0.92	ns	7.01	7.86	7.74
β-catenin	Ctnnb1	1.51	0.01	1.37	0.05	1.11	ns	8.09	8.54	8.69
p120/catenin δ1	Ctnnd1	1.85	0.05	1.14	ns	1.62	ns	5.88	6.07	6.77
γ-catenin/plakoglobulin	Jup	1.95	ns	3.19	0.001	0.61	ns	1.72	3.39	2.68
δ-catenin/catenin δ2	Ctnnd2	0.96	ns	0.65	ns	1.47	ns	2.58	1.97	2.52
ARVCF	Arvcf	10.19	0.001	2.57	ns	3.97	0.001	0.65	2.01	4.00
Plakophilin 2	Pkp2	10.70	0.01	1.13	ns	9.43	0.01	-3.92	-3.74	-0.50
Plakophilin 3	Pkp3	0.08	0.001	0.37	0.001	0.22	0.05	1.45	0.01	-2.16
Plakophilin 4	Pkp4	3.385	0.001	1.61	ns	2.11	0.05	4.54	5.22	6.30

Table S9 - Rho family GAPs and GEFs

Click here to Download Table S9

Table S10 - Rho family actin effectors

Click here to Download Table S10

Table S11. Intermediate filaments

Protein	Gene	C3 / C1	p value	C2 / C1	p value	C3 / C2	p value	Mean Log2 RPM		
								C1	C2	C3
Keratin 7	Krt7	0.08	0.001	0.08	0.001	1.02	ns	-0.38	-4.07	-4.05
Keratin 80	Krt80	0.09	0.001	0.43	0.001	0.21	0.001	2.77	1.55	-0.72
Keratin 86	Krt86	0.11	0.001	0.11	0.001	1.02	ns	-0.86	-4.07	-4.05
Vimentin	Vim	1.12	ns	1.17	0.01	0.96	ns	10.74	10.97	10.91
Nestin	Nes	2657.86	0.001	125.22	0.001	21.22	0.001	-3.80	3.17	7.57
Laminin A	Lmna	6.45	0.001	4.06	0.001	1.59	ns	6.65	8.67	9.34
Laminin B1	Lmnb1	0.08	0.001	0.11	0.001	0.74	ns	8.66	5.44	5.00
Laminin B2	Lmnb2	0.73	ns	0.69	ns	1.06	ns	5.57	5.04	5.12

Table S12 – Differentially expressed genes during IL-4-induced activation

Click here to Download Table S12

Table S13. Core macrophage adhesion proteins, IL-4

Protein	Gene	+IL-4/ -IL-4	p value	Mean Log2 RPM		Function
				-IL-4	+IL-4	
Integrin α1	Itga1	1.06	ns	-1.93	-1.85	Adhesion receptor
Integrin α2	Itga2	1.00	ns	-1.93	-1.94	Adhesion receptor
Integrin α3	Itga3	1.00	ns	-1.93	-1.94	Adhesion receptor
Integrin α4	Itga4	0.63	ns	7.33	6.66	Adhesion receptor
Integrin α5	Itga5	2.42	0.001	6.74	8.01	Adhesion receptor
Integrin α6	Itga6	0.36	0.01	8.30	6.84	Adhesion receptor
Integrin α7	Itga7	1.00	ns	-1.93	-1.94	Adhesion receptor
Integrin α8	Itga8	0.04	0.001	5.59	0.85	Adhesion receptor
Integrin α9	Itga9	0.27	0.01	3.83	1.91	Adhesion receptor
Integrin α10	Itga10	1.00	ns	-1.93	-1.94	Adhesion receptor
Integrin α11	Itga11	1.00	ns	-1.93	-1.94	Adhesion receptor
Integrin αIIb	Itga2b	1.10	ns	-1.69	-1.56	Adhesion receptor
Integrin αD	Itgad	1.00	ns	-1.93	-1.94	Adhesion receptor
Integrin αE	Itgae	1.00	ns	-1.93	-1.94	Adhesion receptor
Integrin αL	Itgal	0.53	ns	7.40	6.49	Adhesion receptor
Integrin αM	Itgam	0.78	ns	10.40	10.05	Adhesion receptor
Integrin αV	Itgav	0.92	ns	7.21	7.10	Adhesion receptor
Integrin αX	Itgax	104.51	0.001	4.68	11.39	Adhesion receptor
Integrin β1	Itgb1	0.92	ns	9.25	9.13	Adhesion receptor
Integrin β2	Itgb2	2.32	0.001	10.40	11.61	Adhesion receptor
Integrin β3	Itgb3	19.60	0.001	1.75	6.04	Adhesion receptor
Integrin β4	Itgb4	1.00	ns	-1.93	-1.94	Adhesion receptor
Integrin β5	Itgb5	1.21	ns	8.05	8.32	Adhesion receptor
Integrin β6	Itgb6	1.00	ns	-1.93	-1.94	Adhesion receptor
Integrin β7	Itgb7	3.33	0.05	1.26	3.00	Adhesion receptor
Integrin β8	Itgb8	12.14	0.001	-1.93	1.67	Adhesion receptor
FAK	Ptk2	2.02	0.05	2.76	3.77	Tyrosine Kinase
Pyk2	Ptk2b	0.87	ns	7.16	6.96	Tyrosine Kinase
Src	Src	5.79	0.001	2.00	4.53	Tyrosine Kinase
Fyn	Fyn	1.95	0.01	5.48	6.44	Tyrosine Kinase
Yes	Yes	1.00	ns	-1.93	-1.94	Tyrosine Kinase
Hck	Hck	0.47	0.001	7.46	6.35	Tyrosine Kinase
Fgr	Fgr	0.79	ns	2.79	2.44	Tyrosine Kinase
Lyn	Lyn	0.42	0.001	7.82	6.55	Tyrosine Kinase
PTPRO	Ptpro	0.43	0.01	7.17	5.95	Tyrosine phosphatase
Paxillin	Pxn	0.76	ns	6.88	6.48	Adaptor
Hic-5	Tgfb1i1	0.63	ns	-1.22	-1.88	Adaptor
Leupaxin	Lpxn	1.86	0.001	6.45	7.34	Adaptor
Vinculin	Vcl	2.60	0.001	5.55	6.93	Adaptor
Zyxin	Zyx	2.82	0.001	7.00	8.50	Adaptor